Metal binding to the surface lipoprotein AdcAI from Streptococcus pyogenes and to the salivary antimicrobial peptide Histatin-5

HONG, YOUNG,JIN

Metal binding to the surface lipoprotein AdcAI from *Streptococcus pyogenes* and to the salivary antimicrobial peptide Histatin-5

Young Jin Hong

Master of Research Thesis
Department of Biosciences
Durham University

2022

Declaration by author

This thesis was composed by myself, that the work contained herein is my own except where explicitly stated otherwise in the text, and that this work has not been submitted for any other degree or processional qualification except as specified.

Acknowledgements

I would like to express my deep appreciation and gratitude to my supervisor Dr Karrera Djoko, for her consistent guidance, wisdom, and enthusiasm throughout this project. I would also like to thank the team, Samantha Firth, Jack Bolton, and Louisa Stewart for always providing practical advice, sparkling ideas, and moral support.

Abstract

The family of human salivary His-rich antimicrobial peptide, histatins, as exemplified by Histatin-5 (Hst5), bind zinc (Zn) and copper (Cu), but the role of metal binding in histatins have not been fully elucidated. Whether Hst5 is involved in nutritional immunity by limiting Zn availability to cause bacterial Zn starvation or by increasing Cu availability to cause Cu toxicity was examined in this study. *Streptococcus pyogenes* or Group A *Streptococcus* (GAS) was used as a model organism as it represents the oral streptococci that make up approximately 60 % of the oral microbiome. The metal binding affinity of Hst5 was measured by equilibrium competition assays using colourimetric probes and was compared against the high-affinity Zn uptake protein AdcAI from GAS. These experiments confirmed that Hst5 binds Zn weakly, and it does not strongly influence Zn availability. In addition, Hst5 cannot compete for Zn binding with AdcAI, which has an affinity that is 8 orders of magnitude higher than that of Hst5. In contrast, Hst5 has a high affinity for Cu and therefore influences the Cu availability. However, it does not promote Cu toxicity in GAS by delivering excessive Cu into the cytoplasm. It rather protects from the accumulation of intracellular Cu in Δ*copA* mutant strain that is hypersensitive to increased Cu availability due to the loss of ability to export intracellular Cu. Whether Cu induces Cu starvation in Cu-requiring microbes remains unsolved, but this study has opened the possibility of Hst5 providing a buffering effect from metal toxicity to maintain a healthy oral microbiome.

Table of Contents

List of abbreviations

AMP	Antimicrobial peptide
ATCUN	Amino-terminal Copper and Nickel binding
BCA	Bicinchoninic acid
BCS	Bathocuproine disulfonic acid
CDF	Cation diffusion facilitator
CV	Column volume
EDTA	Ethylenediaminetetraacetic acid
ESKAPE	*Enterococcus faecium, Staphylococcus aureus, Klebsiella pneumoniae, Acinetobacter baumannii, Pseudomonas aeruginosa, Enterobacter spp.*
FZ3	FluoZin3
GAS	Group A *Streptococcus*
Hst5	Histatin-5
ICP MS	Inductively coupled plasma mass spectrometry
IPTG	Isopropyl β-D-1-thiogalactopyranoside
ITC	Isothermal titration calorimetry
LB	Lysogeny broth
LIC	Ligation independent cloning
MF2	MagFura2
MOPS	3-(*N*-morpholino)propanesulfonic acid
NETs	Neutrophil extracellular traps
NTA	Nitrilotriacetic acid
OD	Optical density
PAR	4-(2'-Pyridylazo)resorcinol
PBS	Phosphate-buffered saline
PCR	Polymerase chain reaction
PES	Polyethersulfone
ROS	Reactive oxygen species
SAAP	Asp-rich anionic antimicrobial peptide
THY	Todd-Hewitt Broth with 2% Yeast Extract

TPEN	N,N,N’.N’-Tetrakis(2-pyridylmethyl)ethylenediamine
WT	Wild type

1. Introduction

1.1 Metals in life

Metals are essential micronutrients for life. It is estimated that approximately half of all proteins contain metals and up to one third of all enzymes require metals to function. Metal ions can act as catalysts and enable chemical reactions to take place. Key cellular processes such as transcription [1], translation [2], carbon metabolism [3], oxidative phosphorylation [4], and response to oxidative stress [5] all rely on metalloproteins. Iron (Fe), being a redox-active metal, is used by proteins that carry out redox reactions or electron transfer, for example as part of iron-sulfur (Fe-S) clusters in the respiratory and electron transport chain [6]. On the other hand, zinc (Zn) is a non-redox metal that often acts as a Lewis acid catalyst and plays a crucial role in hydrolysis reactions, such as in metallo-β-lactamases, which use Zn to activate a water molecule (H_2O) to hydrolyse β-lactam rings and inactivate β-lactam antibiotics [7]. Metal ions also play important roles in stabilising protein structures. For example, Zn is present in the Zn finger domains in mammalian cells to achieve specific DNA binding [8]. Another important physiological role of metal ions is in cell signalling. Magnesium (Mg) is one of the most recognised signalling molecules along with calcium (Ca), and Zn and copper (Cu) are also known to take part in signal transduction within the nervous system [9, 10].

1.2 Metal homeostasis

Metalloproteins and metalloenzymes are highly specific for their cognate metals and only the cognate metal provides the correct activity. However, metal selectivity is a major problem in cells as most proteins favour binding to the wrong metal rather than its cognate metal. The order of affinities of metal binding to proteins is described by the Irving-Williams series (Figure 1) [11]. The Irving-Williams series describes that proteins bind to metals higher up in the series, such as Cu(II) (or Cu(I)), with higher affinities compared to metals lower down in the series, such as cobalt (Co(II)). Thus, given the same availability of Co and Cu, the Co-binding protein will bind the wrong metal.

Cells have evolved a mechanism to help proteins to bind correct metals. They do so by regulating intracellular metal availability. Metal availabilities in cells are typically maintained in the reverse order

of the Irving-Williams series, *i.e.* tighter binding metals are maintained at lower availabilities [12]. Cells generally maintain the availabilities of tighter binding metals below the threshold of mismetalating wrong proteins, but above the threshold for metalating their cognate proteins. By contrast, weaker binding metals are kept at higher availabilities, so that they can bind their cognate proteins but will not bind others as they are outcompeted by tighter binding metals. Intracellular metal availabilities are regulated by metal-sensing transcriptional regulators that upregulate or downregulate the production of metal import, storage, trafficking, and export proteins [13]. Cells also contain molecules that are considered for their capacity to bind metals and act as metal buffers, such as small organic molecules like amino acids, nucleotides, and peptides. Together, these components form the cellular systems for metal homeostasis.

Mn(II) < Fe(II) < Co(II) < Ni(II) < Cu(II) > Zn(II)

Figure 1 Irving-Williams series

1.3 Metal dyshomeostasis

The dyshomeostasis of metal ions can lead to various cellular defects. Since many essential cellular processes depend on the presence of metal ions, metal deficiency leads to inefficient cellular metabolism, but the specific consequence depends upon which metal ion is lacking in the cell. For example, Zn starvation can lead to decreased protein synthesis as a result of inactive RNA polymerase [14] and ribosomes [15], and disruption of Zn-finger domain transcriptional factors [16]. Fe deficiency can perturb energy metabolism by decreasing the activity of heme-dependent respiratory oxidases [17], Fe-dependent ribonucleotide reductases that catalyse DNA synthesis and repair, and Fe-S cluster dehydratases that catalyse branched-chain amino acid synthesis [18]. Cu limitation can also reduce respiratory activity as a result of decreased activity of the heme-Cu oxidases. Cu limitation can also suppress cellular defensive mechanisms, for example by decreasing the activity of the Cu,Zn-dependent superoxide dismutases [19] that are involved in neutralising toxic reactive oxygen species (ROS).

Conversely, an excess of metal ions can overwhelm the normal metal homeostasis machinery and lead to metal toxicity. An excess of redox-active metals such as Fe or Cu can promote generation of ROS *via* Fenton or Fenton-like reactions (Scheme 1) [20, 21]. These ROS are highly toxic to the cell, since they can oxidise essential cell components such as nucleic acids, proteins, and lipids, leading to oxidative stress. An excess of metals, including those that are not redox-active, can also promote toxicity *via* adventitious binding or mismetalation of proteins, leading to incorrect folding and conformation, and the failure to establish the correct function of the protein or catalyse the correct reactions. This phenomenon is particularly well described in the case of Cu [22]. As mentioned earlier, Cu sits at the top of the Irving-Williams series, and it is thus a competitive metal for binding to proteins. An excess of Cu is known to outcompete Fe from 4Fe-4S cluster enzymes, leading to destruction of the clusters and inactivation of the enzymes [23]. There is also evidence that Cu can inactive Zn- and Mn-dependent enzymes [24, 25] or enzymes that contain potential metal-binding ligands such as Cys or His in the active site [26].

Scheme 1. Illustration of Fenton or Fenton-like reactions of Fe and Cu.

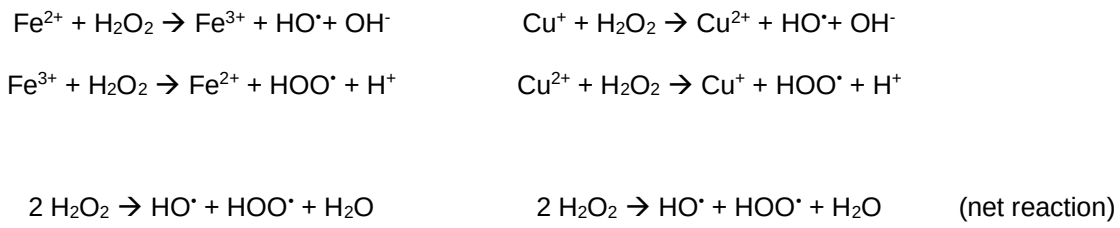

1.4 Metals in host-bacteria interactions

It is now well established that the control of metal availability is important during host-bacteria interactions. In the innate immune response to infection, vertebrate hosts can secrete metal-chelating molecules that limit metal availability to bacteria. This phenomenon is called nutritional immunity [27]. One well studied example of a host metal-chelating molecule is calprotectin. Calprotectin is a member of the S100 protein family. This protein is composed of the S100A8 (α) and S100A9 (β) proteins, forming a heterodimer (αβ) or heterotetramer ($\alpha_2\beta_2$) [28]. Calprotectin is released by neutrophils in neutrophil extracellular traps (NETs). It was first identified to bind Zn and Mn at the HXXXH site [29] and His_6

binding site (PDB: 4XJK) [30], respectively. Calprotectin is also known to bind Fe at the His_6 site [31] and Cu, presumably at the His_6 site [32]. *In vitro* treatment with calprotectin inhibits growth of diverse bacteria and this phenotype is often associated with the depletion of cellular Zn and Mn content [33], although there is also evidence that this protein can deplete Fe or Cu [31, 32]. *In vivo* studies using animal models of infection indicate that calprotectin-deficient mice are more prone to infection by *Staphylococcus aureus* compared to wild-type mice [33]. Other examples of host metal-chelating molecules include transferrin and lactoferrin, which bind Fe(III), as well as siderocalin, which binds *holo*-siderophores [34]. The circulating levels of these host proteins in the serum are known to increase in response to infection, in a process known as hyperferremia, leading to decrease in Fe availability in the whole animal and Fe limitation in the invading pathogens.

Although the concept of nutritional immunity was originally developed to describe a decrease in host metal availability in response to infection, it is now understood that the host innate immune system can also increase metal availability. This process is best understood in the case of Cu. ATP7A is a major Cu-translocating P_{1B}-type ATPase in vertebrate hosts. This transporter is found in all cell types, including macrophages, which are innate immune cells. ATP7A is usually located in the trans-Golgi membrane, but in response to infection, this transporter is trafficked to the phagosomal membrane instead. This transporter is thought to increase Cu availability in the phagosome, where it can amplify the antimicrobial activity of ROS from the respiratory burst. Consistent with this idea, macrophages from ATP7A-deficient mice show reduced antimicrobial activity [35].

Since changes in metal availability are important mechanisms of the host innate immune response, it is not surprising that bacterial responses to changing metal availability are considered major virulence determinants for many clinically significant pathogens. Mutant strains lacking pathways for Zn, Mn, or Fe uptake often display reduced virulence in animal models of infection [36]. *In vitro*, these mutant strains are often more sensitive to growth inhibition by the relevant host metal-chelating proteins when compared with wild-type bacteria. Similarly, mutant strains lacking pathways for Cu efflux also often show reduced virulence in animal models of infection [36].

1.5 Antimicrobial peptides

Antimicrobial peptides (AMPs) are also key components of the host innate immune system [37]. AMPs are short peptides, generally between 12 to 50 amino acids long, and often cationic. They exhibit a wide range of inhibitory effects against microbial pathogens including bacteria, fungi, viruses, and parasites. AMPs can be classified according to whether or not they act on microbial membranes. The membrane-targeting or membrane-permeabilising AMPs can be further sub-categorised depending on the specific modes of action, but all cause formation of membrane pores or channels, inducing leakage of cytoplasmic molecules such as ATP and K^+, and the concomitant influx of water, which lead to cell lysis. By contrast, non-membrane permeabilising AMPs usually become internalised by the target microbes without damaging the microbial membranes. Once in the cytoplasm, these AMPs can inhibit cellular metabolism such as transcription, translation, nucleic acid biosynthesis and cell division [38].

A subset of AMPs is metal-dependent. The metal ion can enable the antimicrobial function of the AMP. Alternatively, the AMP can modulate metal availability in a manner that resembles nutritional immunity. For example, Cys-rich defensins from humans [39] and His-rich defensins from plants [40] can bind Zn, providing resistance to metal toxicity. The metal-bound form of defensins may also have antimicrobial function [39, 41]. Piscidins, which are found in fish, are also rich in His residues and they have the characteristic Amino-terminal Copper and Nickel binding (ATCUN) motifs known for Cu(II) and Ni(II) binding. Binding of Cu(II) ions enhance the antimicrobial activity of piscidins, and allow these peptides to catalyse ROS formation, DNA damage, and lipid peroxidation [42]. Calcitermin, a Zn-binding AMP from the human nasal cavity, becomes activated in acidic conditions, indicative of inflammation. Amylin and semenogelin, from the islet of Langerhans and sperms of human, respectively, and Asp-rich anionic AMPs (SAAPs), derived from sheep, also have activities that are enhanced by Zn, although the specific mechanism of action is yet to be determined [43]. Similarly, microplusin is a His-rich, Cu binding AMP from ticks, which is thought to promote Cu starvation in bacteria and fungi [44] *via* a mechanism that remains to be defined.

1.6 Histatin-5

Of interest in this study is Histatin-5 (Hst5), a metal-binding, His-rich AMP, which is found in the saliva of higher primates, including humans [45]. Hst5 is the major AMP among many His-rich AMPs in saliva, all of which are derived by proteolytic degradation from only two parent peptides, namely Histatin-1 and Histatin-3. Like other AMPs, the salivary His-rich AMPs are thought to play a role in the host innate immune defence. Hst5 has a well described *in vitro* antimicrobial activity against opportunistic oral fungal pathogens such as *Candida albicans.* It is also known to be affective against ESKAPE pathogens [46].

Unlike many cationic AMPs, Hst5 does not appear to fold into a helical structure in aqueous solutions, but in membrane-like environment, such as in $(CD_3)_2SO_4$ solution, it does retain an alpha helical structure [47]. However, this is unusual of membrane targeting AMPs, thus thought to have an alternative mechanism of action. It was observed that Hst5 binds to the fungal membrane proteins and internalised into the cytoplasm *via* energy-dependent pathways [48]. It is speculated to cause toxicity intracellularly by generating ROS, but how it encounters its target and induce toxicity in multiple pathways is not fully elucidated [49, 50].

Metal binding to Hst5 is relatively well characterised. This AMP is 24 amino acids long with multiple metal binding motifs (Figure 2). Hst5 is thought to bind up to 2 Zn atoms at each of the two His-Glu-X-X/His-His motif with dissociation constant (K_D) of $K_D = 1 \times 10^{-5}$ M and 1×10^{-4} M, which were determined by isothermal titration calorimetry (ITC) [51]. The N-terminal ATCUN motif is known to bind Cu(II) as well as Ni(II). Based on competition experiments with the Cu(II) ligand nitrilotriacetic acid (NTA), the affinity of the ATCUN site to Cu(II) was determined to be $K_D = 7.94 \times 10^{-12}$ M, which is typical of ATCUN motifs [52]. Mutation of the ATCUN His3 to an Ala reduced this affinity such that it could no longer be measured by competition with NTA, confirming the role of the ATCUN His in binding Cu(II). Finally, the two *bis*-His motifs are thought to bind one Cu(I) each with an affinity of $K_D = 2.51 \times 10^{-8}$ M, which was determined by competition with the Cu(I) ligand ferrozine [52]. Mutation of both His residues (His7, His8) to Ala resulted in the loss of Cu(I) binding such that the peptide could not compete with ferrozine. Additional reports suggest that Hst5 can also bind up to 10 Fe atoms at unknown binding sites [53].

To date, the precise roles of metal binding by Hst5 are unknown. Conklin et al. showed that adding Cu into the culture medium decreased the EC_{50} value of Hst5 against *C. albicans* (the concentration of Hst5 required to kill 50% of the pathogen), suggesting that Cu enhances the antifungal activity of Hst5 [52]. It was hypothesised that the Cu(II)-Hst5 complex can catalyse production of ROS, once the *holo*-AMP localises to the target and promote oxidative damage, but whether this target is the cell membrane, DNA, or an organelle is not clear.

The relationship between the antimicrobial activity of Hst5 and Zn has also been studied. However, there are conflicting reports that the antifungal activity can be both increased and decreased by Zn. Norris et al. observed that the addition of Zn enhances fungicidal activity of Hst5 against *C. albicans* and leads to immediate leakage of ATP out of the cell. This enhancement appeared to depend on the concentration of Zn [54]. By contrast, Puri et al. observed that adding up to 1 equivalent of Zn does not affect the antimicrobial activity of Hst5 but adding 2 equivalents of Zn reduces the killing activity [53]. Therefore, whether Zn has a positive or negative impact on the antifungal activity of Hst5 is currently unclear. However, it is worth noting that the solubility of Hst5 decreases in the presence of Zn concentrations above the ratio of 2:1 Zn:Hst5. Therefore, the reduced killing seen in Puri et al., may be due to the precipitation of Hst5, which is observed in the Norris et al. study.

There is currently a major gap in knowledge regarding the role of metal binding in the function of Hst5. In particular, whether or not Hst5 contributes to nutritional immunity has not been investigated. Given the ability of this AMP to bind Zn and Cu, it is hypothesised that Hst5 promotes Zn and/or Cu starvation in invading pathogens, similar to the action of calprotectin. Alternatively, Hst5 may promote Zn and Cu toxicity, similar to the action of ATP7A.

Figure 2 Sequence of Hst5 with conserved metal binding motifs highlighted [54].

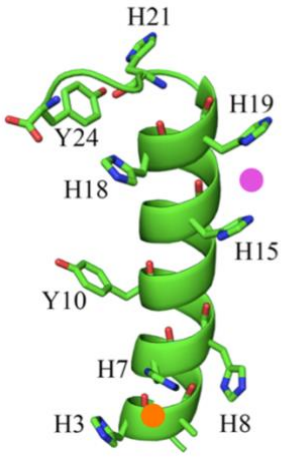

Figure 3 PEP-FOLD model of Hst5. The speculative binding site for Zn shown in pink and Cu(II) in orange [55].

1.7 *Streptococcus pyogenes*

Streptococcus pyogenes is a Gram-positive bacterium that is an obligate human pathogen which causes strep throat, impetigo, skin infection and may cause more serious infections such as pneumonia and streptococcal toxic shock syndrome [56]. *S. pyogenes* was selected as the model organism for studying the metal-dependent effect of Hst5 because it is a pathogen that requires Zn for growth and pathogenicity and it colonises the oropharynx, where it encounters Hst5 in swallowed saliva. *S. pyogenes* has a well-known Zn homeostasis system, which resembles the system from *S. pneumoniae,* and which is highly conserved among the oral streptococci [57].

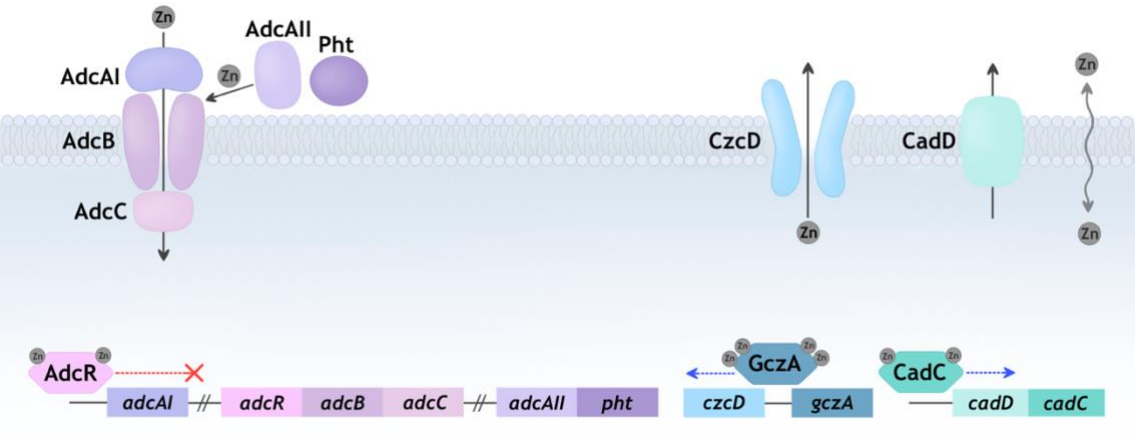

Figure 4 Zn homeostasis system of *S. pyogenes.* The transcriptional regulators AdcR, GczA and CadC homodimers but depicted as a single molecule.

1.8 Zn homeostasis in *S. pyogenes*

(A) The Zn sensors

The response of *S. pyogenes* to Zn starvation is controlled by AdcR, a MarR family transcriptional co-repressor. AdcR is a homodimer, and it contains two Zn sites in each monomer (4 Zn per homodimer), known in the literature as Site 1 and Site 2. Site 1 is the primary allosteric Zn-sensing site while Site 2 has an unknown function. The affinities of both sites have not yet been measured, but they are likely comparable to those of AdcR from *S. pneumoniae* (54% identity, 76% similarity with *S. pyogenes* AdcR). Based on competition experiments with the fluorometric Zn ligand MagFura-2 (MF2), Site 1 of *S. pneumoniae* AdcR binds Zn tightly with a K_D of 7.4×10^{-13} M [58]. The Site 1 affinity of AdcR is approximately 2 orders of magnitude lower than other Zn sensors like Zur in *E. coli*, which has femtomolar (10^{-15} M) affinity [59].

In response to Zn sufficiency, cytoplasmic Zn binds to Site 1 of AdcR. This Zn-bound form of AdcR binds DNA upstream of the *adc* operon and represses transcription of the Zn import genes, namely *adcABC*, *adcAII* and *pht* [60]. AdcABC is an ABC-type Zn import transporter that consists of the transmembrane permease AdcB and the cytoplasmic ATP hydrolysis domain AdcC. Two solute binding lipoproteins, namely AdcAI and AdcAII can acquire Zn from the extracellular space and donate Zn to AdcBC to be imported into the cytoplasm. Pht is a His-rich protein that is thought to be co-localised on the cell surface along with AdcAI and AdcAII, which is thought to donate Zn to the AdcABC system, though its precise role is yet unclear [61] (Figure 4).

Conversely, Zn limitation promotes dissociation of Zn from AdcR and induces a conformational change that leads to dissociation *of apo*-AdcR from its binding site on the *adc* promoter. This allows expression of the Zn import genes and restoration of intracellular Zn availability. Consistent with their roles in Zn uptake, mutant strains lacking the *adcAI* had attenuated growth in Zn-depleted media [61].

The response to excessive Zn is controlled by two sensors, GczA and CadC. GczA is a TetR family transcriptional de-repressor of *czcD* [62], which is a homodimer that binds two Zn ions per monomer. The dissociation constants for the *S. pyogenes* sensor are unknown, but the *S. agalactiae* homologue (77 % identity and 90 % similarity with *S. pyogenes* GczA) was shown to bind Zn with affinity of $K_{DZn1} \leq$

10^{-9} M and K_{DZn2} = 4.08 × 10^{-9} M, as determined by competition assays with MF2 [63]. The *apo*-form of GczA binds to DNA but in response to Zn excess, Zn metalates the sensing site of GczA, releasing it from the DNA, leading to expression of *czcD* and production of the Zn-exporting cation diffusion facilitator family transporter CzcD (Figure 4). Consistent with its role in Zn efflux, *S. pyogenes* mutant strains lacking the *czcD* gene had reduced survival in the neutrophil [62]. The CadCD system is not yet well described. Sequence analysis suggests that CadC is an ArsR/SmtB family transcriptional activator [64] and CadD is a CadD family transporter. The *cadCD* operon is annotated on the *S. pyogenes* genome as a cadmium efflux system. However, preliminary work in the Djoko lab suggests that it may act as a Zn efflux system in *S. pyogenes*, based on induction of both genes in response to excess Zn and sensitivity of the Δ*cadCD* mutant strain to excess Zn. When compared with *czcD*, the *cadCD* operon was induced by higher concentrations of added Zn. Thus, CzcD is likely to be the primary Zn efflux pump in *S. pyogenes*.

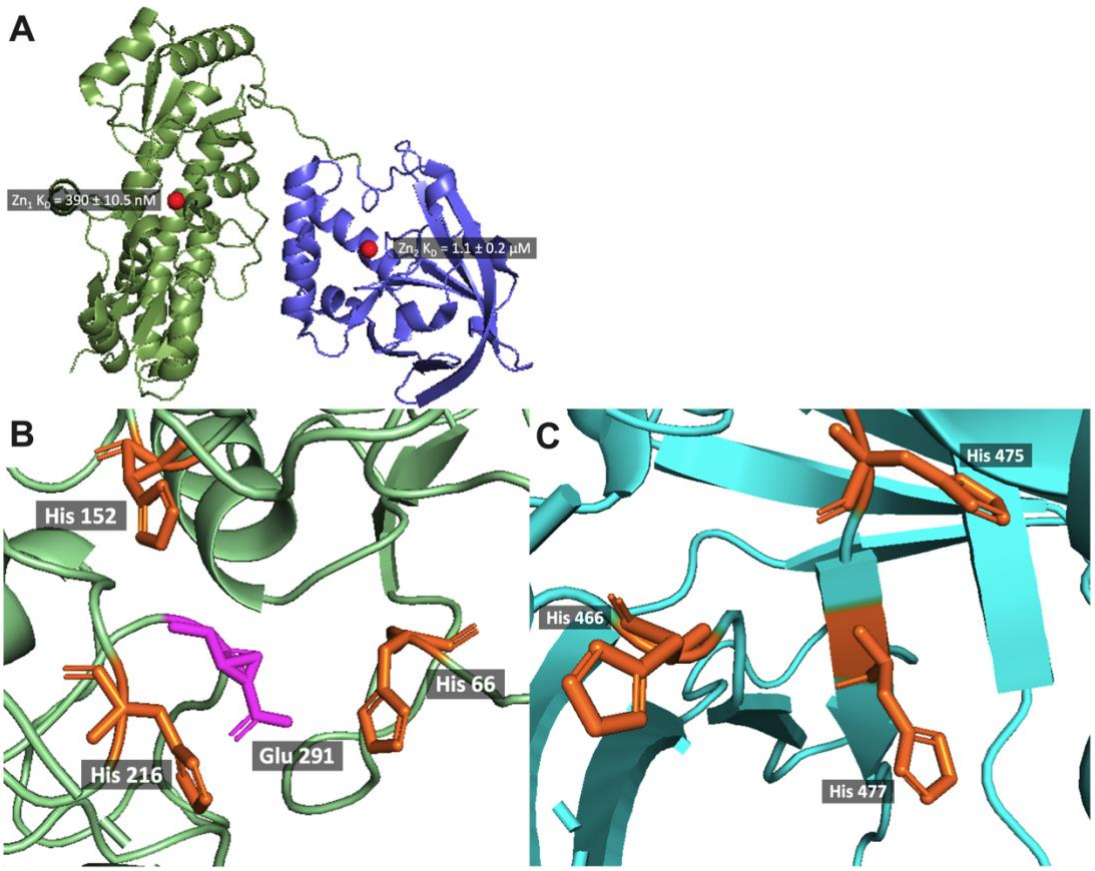

Figure 5 A *S. pneumoniae* AdcAI crystal structure (RCSB PDB: 7JJ9) (green: N-terminal domain, blue: C-terminal domain, red spheres: Zn bound). **B** Predicted Zn binding ligand of *S. pyogenes* N-terminal domain. **C** Predicted Zn binding ligand of *S. pyogenes* C-terminal domain.

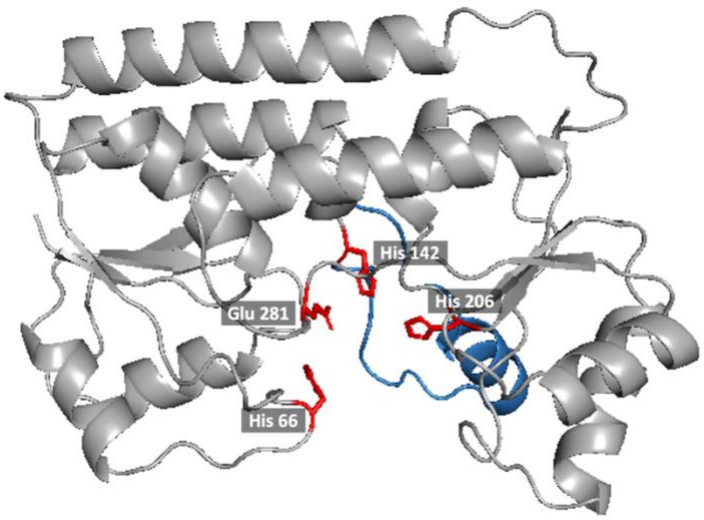

Figure 6 *S. pyogenes* AdcAII 3D modelling structure using Phyre2 (red: Zn binding ligands, blue: closing loop).

(B) The Zn uptake lipoproteins AdcAI and AdcAII.

AdcAI is a double-domain Zn binding lipoprotein that is exposed at the surface of *S. pyogenes*. Based on sequence alignment with *S. pneumoniae* AdcAI, whose X-ray crystal structure has been solved (RCSB PDB: 7JJ9) [65], the *S. pyogenes* AdcAI likely has two Zn-binding sites: one at the N-terminal domain (green in Figure 5A) and one at the C-terminal domain (blue in Figure 5A) [66]. The affinities of each Zn binding site have been measured by ITC, either in the full-length protein containing both domains, or individually in variant and truncated proteins that contain only one of the domains. These measurements revealed a K_D value between 1.1 to 2.6 µM for the C-terminal domain, and between 93 to 390 nM for the N-terminal domain [66].

AdcAII is a homolog of AdcAI, and it contains only a single Zn binding site (Figure 6). The *adcAII* gene is co-expressed as an operon with *pht,* and the proteins, AdcAII and Pht, are also thought to be co-located on the bacterial surface.

Both AdcAI and AdcAII are thought to be essential for Zn uptake, based on growth analyses of the *S. pneumoniae ΔadcAI ΔadcAII* mutant strain. This mutant strain does not grow in Zn-depleted culture media, consistent with the loss of the Zn uptake system. Single deletions of either *adcAI* or *adcAII* did not completely abolish Zn import in *S. pneumoniae* [67], suggesting the overlapping role of the two proteins in Zn uptake. In *S. pyogenes*, the deletion mutant of *adcAI* results in inhibited growth in Zn limited conditions compared to the *S. pyogenes* wild type (WT). However, there are varying results of growth assays of *adcAII* deletion mutants in *S. pyogenes*. Some studies report that the single mutants of either the *adcAI* or *adcAII* is sufficient to inhibit growth while some studies showed a greater inhibition of growth in Δ*adcAI* than in Δ*adcAII* and only the double mutant Δ*adcAI* Δ*adcAII* induced complete growth inhibition [61, 68]. Nonetheless, both genes are upregulated in Zn deficiency, suggesting that both AdcAI and AdcAII plays a role in Zn acquisition during Zn starvation, although the precise mechanism of AdcAII remains poorly understood.

Mice models infected with *S.pyogenes* Δ*adcAI* Δ*adcAII* developed skin lesions slower than the mice infected with *S. pyogenes* WT, and the lesions developed were significantly smaller [68]. In addition, complementation with the full length *adcAI* gene from *S. pyogenes* restored growth of the *S. pneumoniae ΔadcAI ΔadcAII* mutant back to wild type levels [66]. These studies show the importance of Zn acquisition and the role of AdcAI and AdcAII in group A *Streptococcus* (GAS) infection.

(C) The Zn efflux transporter CzcD

CzcD is a cation diffusion facilitator (CDF) family Zn transporter and is the primary Zn export pump in *S. pyogenes.* CDF transporters are dimeric with N-terminal helical transmembrane domains and C-terminal domains which face the cytoplasm to bind intracellular metal ions. The best characterised CDF is the Zn and Fe transporting YiiP in *E. coli*, homologous to the *Streptococcal* CzcD [69]. In both *S. pyogenes* and *S. pneumoniae*, deletion of *czcD* results in increased sensitivity to growth inhibition by supplemental Zn in the culture media [62, 70]. Inductively coupled plasma mass spectrometry (ICP MS) analyses of total cellular metal levels also revealed that the ∆*czcD* mutant strains contain significantly higher levels of Zn compared to the wild type parent strains, particularly when the growth media are supplemented with extracellular Zn. It was further shown that the ∆*czcD* mutant of *S. pyogenes* had a lower survival rate in neutrophil intracellular killing assays. This lower survival was rescued by the

addition of a Zn chelator, N,N,N'.N'-Tetrakis(2-pyridylmethyl)ethylenediamine (TPEN), indicating that the accumulation of intracellular Zn inside the neutrophils is responsible for the enhanced killing in *S. pyogenes* [62]. This work highlights that, in addition to Zn limitation, which is promoted by calprotectin in NETs outside the neutrophils, pathogenic bacteria also encounter Zn toxicity, which occurs inside the neutrophils *via* mechanisms that are not yet understood.

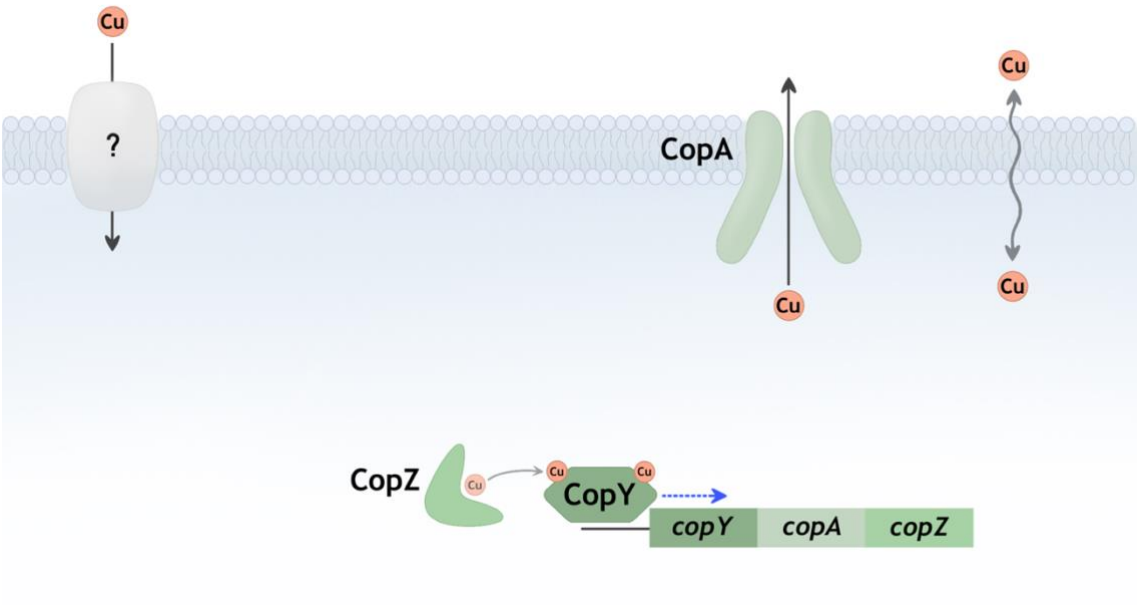

Figure 7 Cu homeostasis system of *S. pyogenes.*

1.9 Role of Zn homeostasis in *S. pyogenes* pathogenesis

As well as survival, the Zn homeostasis in *S. pyogenes* is crucial for pathogenesis. The mutation of His66 to Ala in the metal binding site of AdcAII (also known as Lmb or Lsp) had reduced ability to cause disease in skin tissue. Also, the *S. pyogenes* Δ*adcAII* mutant had attenuated virulence in mice models with significantly reduced development of lesions [71]. These studies show the importance of the Zn import system in the virulence of *S. pyogenes.* Similarly, excessive Zn was also shown to inhibit the phosphoglucomutase in the nucleotide sugar metabolic pathway. This pathway produces the precursors of hyaluronic acid capsule of *S. pyogenes* [72], which plays critical roles in immune invasion by providing resistance to phagocytosis [73]. Also, studies have shown that excessive Zn inhibits the *S. pyogenes* Cys protease SpeB [74], which cleaves the host proteins including fibronectin, fibrinogen and immunoglobulins, as well as bacterial proteins like the M protein to prevent phagocytosis [75].

1.10 Cu homeostasis in *S. pyogenes*.

The genome of *S. pyogenes* does not encode for any recognisable Cu-dependent proteins or enzymes and therefore this bacterium is not thought to use Cu as a nutrient. Nevertheless, Cu can still enter the *S. pyogenes* cytoplasm, likely via non-specific uptake. To avoid potential Cu toxicity, *S. pyogenes* possesses the *copYAZ* operon for Cu efflux, which is regulated by the Cu-sensing transcriptional regulator CopY [76] (Figure 7). CopY is a CopY/TcrY family transcriptional repressor which binds 1 Cu per monomer (2 Cu per homodimer). The *S. pneumoniae* CopY (with 40-50 % identity to *S. pyogenes* CopY) has affinity of K_D = 2.51 × 10^{-17} M to Cu(I) that was measured by competition assays with bathocuproine disulfonic acid (BCS) [77]. During conditions of low intracellular Cu availability, the sensor site of CopY is thought to bind Zn. This Zn-bound form of CopY binds to the promoter region of the *copYAZ* operon and represses transcription. In response to an increased intracellular Cu availability, Zn is displaced by Cu. This induces a conformational change and leads to de-repression of transcription. CopA is a P_{1B}-type ATPase that exports Cu(I) out of the cytoplasm to the extracellular space. CopZ is likely to be a cytoplasmic Cu(I)-binding metallochaperone (Figure 5).

How Cu enters the cytoplasm of *S. pyogenes* is unknown. This organism does not possess known Cu import systems such as the major facilitator superfamily transporter CcoA [78] and it does not encode a system for the biosynthesis, export, and uptake of Cu-binding siderophores (chalkophores) such as methanobactin [79]. Pathways of non-specific Cu uptake into bacteria remain poorly characterised, but a recent study using *Staphylococcus aureus* suggests that the Mn-import ABC transporter system MntABC may promote Cu uptake [80]. The mechanisms for this Cu uptake are not yet defined, but, like *S. aureus*, *S. pyogenes* also possesses an MntABC-like import system for Mn, named MtsABC [81] that may promote Cu uptake. As described earlier, the homologous AdcAI/AdcAII-AdcBC system imports Zn, but whether it participates in Cu uptake has not been investigated.

1.11 Role of Cu homeostasis in *S. pyogenes* pathogenesis

Cu homeostasis is also important in the pathogenicity of *S. pyogenes* because this organism encounters elevated levels of Cu during infection. For example, the Cu level in the blood is low compared to the lungs and respiratory tracts, where the Cu level is much higher. Expression of the *cop* operon in *S.*

pneumoniae that was isolated from the lungs and nasopharynx tissue was shown to be higher compared to *S. pneumoniae* isolated from the blood. Consistent with this, studies with mouse model of infections suggest that a mutant strain of *S. pneumoniae* lacking the *copA* gene had reduced survival compared to the wild type in the mice lungs and nasopharynx, but not in the blood [82]. These findings using *S. pneumoniae* are similar to those using *S. pyogenes*. The CopA protein from both organisms share 44-54% amino acid sequence similarity and identity. Growth of *S. pyogenes copA* deletion mutants were more susceptible to growth inhibition in additional Cu in the medium with higher accumulation of intracellular Cu. However, the deletion of *copA* does not cause the loss of virulence in a mouse model infection, which was suggested to be due to the buffering of extracellular Cu in the study of Stewart et al. [83]. Nonetheless, the *cop* operon is upregulated in *S. pyogenes* in increased extracellular Cu in the growth media to provide resistance from Cu poisoning. It was also shown that the *copA*-deficient *E. coli* recovered growth in excessive Cu when it was complemented with the *S. pyogenes cop* operon, confirming that CopA is essential in resistance to Cu toxicity [76].

1.12 Aims and Hypothesis

To date, the role of metal binding in the function of histatin AMPs from human saliva is poorly defined. Whether or not the histatins exert an antibacterial activity against *S. pyogenes*, which colonises the human throat, is also unknown. Given the known roles of some metal-binding immune proteins in nutritional immunity and in influencing metal availability during the immune response to infection, histatins are likely to play a similar role in the nutritional immune response against *S. pyogenes*.

Therefore, the specific hypotheses of this project are:

1. Histatins sequester Zn from *S. pyogenes* and promote Zn limitation.
2. Histatins supply Cu to *S. pyogenes* and promote Cu toxicity.

To test these hypotheses, this project aims to:

1. Measure the Zn and Cu-binding affinities of histatin-5 (Hst5) as a model histatin and identify the metal binding motifs.

2. Measure the Zn-binding affinities of the extracellular Zn binding protein of the import system of *S. pyogenes*, AdcAI and AdcAII, to compare with Hst5.
3. Evaluate the effects of Hst5 directly on the growth of *S. pyogenes* in the presence of Zn or Cu.

2. Materials and Methods

All materials were supplied by Sigma-Aldrich, using analytical grade unless otherwise stated. Where required, deionised ultrapure (MilliQ) water was used in making buffer, metal stocks, probe stocks and media.

2.1 Cloning, expression, and purification of AdcAI and AdcAII

AdcAI and AdcAII were produced by cloning the *adcAI* and *adcAII* genes amplified without the first 60 and 87 base pairs, respectively, using the genomic DNA of *S. pyogenes* M5005 as a template (GenBank: CP000017.2). Primers were designed (Table 1) to attach overhangs to the genes amplified for LIC cloning into the pSATL plasmid using StuI. The pSATL plasmid has a His_6-SUMO tag insert before the site of gene insert for purification. The cloned plasmids were verified by Sanger sequencing and heat shock transformed into the expression host *E. coli* BL21 Rosetta 2(DE3).

Table 1 List of primers used in this study.

Amplicon name	**Primer name**	**Sequence (5'→3')**	**Locus Tag of target gene**	**Amplicon size (bp)**
Overexpression primers				
adcAI	adcAI-F	CAACAGCAGACGGGAGGTACTCAGGCAAAACAAGTCTTAGC	M5005_Spy0543	1488
	adcAI-R	GCGAGAACCAAGGAAAGGTTATTAATGAGCATTGATTTCTTGGGC		
adcAII	adcAII-F	CAACAGCAGACGGGAGGTACGCAAGGCATGTCAGTTGTAAC	M5005_Spy_1711	834
	adcAII-R	GCGAGAACCAAGGAAAGGTTACTTCAACTGTTGATAGAGCACTTCC		
Sanger Sequencing primers				
adcAI	T7-R	GCTAGTTATTGCTCAGCGG	pSATL::*adcAI*	-
	adcA(GAS)-qPCR-R1	CATGGTTGTGTCCTTCTTCGC		-
	adcA(GAS)-qPCR-F2	ACCATGCTTTTGACCCACAC		-
adcAII	T7-R	GCTAGTTATTGCTCAGCGG	pSATL::*adcAII*	-
	adcAII(GAS)-qPCR-R2	GGGTCATAAAGTGTCGCAGG		-

Table 2 List of plasmids used and generated in this study.

Plasmid name	Description	Source
pSATL	Empty vector for overexpression	T Blower (Durham)
pSATL-adcAI	Plasmid for overexpression of AdcAI, where the *adcAI* gene is subcloned between 6His-SUMO and T7 Terminator.	This work
pSATL-adcAII	Plasmid for overexpression of AdcAI, where the *adcAII* gene is subcloned between 6His-SUMO and T7 Terminator.	This work

To overexpress the protein, transformants were plated on to LB agar containing ampicillin and chloramphenicol. Fresh colonies were harvested to inoculate LB broth containing ampicillin and chloramphenicol to an optical density at 600 nm (OD_{600}) of 0.01. The total volume of inoculated LB broth was 2 L, 500 mL in 2 L baffled flasks. Where required, ampicillin and chloramphenicol were added to 100 µg/mL and 33 µg/mL, respectively.

Cultures were shaken (37 ^{o}C, 180 RPM) until OD_{600} reached 0.6 – 0.8 and Isopropyl β-D-1-thiogalactopyranoside (IPTG) was added to a final concentration of 0.1 mM, to induce the expression of the proteins. After shaking the culture for 16 hours at 20 ^{o}C, bacterial cells were harvested by centrifugation (4000 x g, 4 ^{o}C) and resuspended in buffer A500. Cells were lysed by sonification (40 kPsi), centrifuged (20000 x g, 4 ^{o}C) and filtered through a 0.46 µm Polyethersulfone (PES) membrane filtration unit.

Clarified lysates were loaded onto a HisTrap™ HP 5 mL column (Cytiva). Then the column was washed with 10 column volume (CV) of buffer A500 and eluted with 3 CV of buffer B100 and 3 CV of buffer B100 2X imidazole, collecting in 1 mL fractions. Fractions containing the protein were immediately loaded onto a HiTrap™ Q HP 5mL column (Cytiva). Then the column was washed with 10 CV of buffer A100, and the protein was eluted by a stepwise gradient of 150 mM, 200 mM and 250 mM NaCl with buffer A100 and C1000 mixed. The recipes of buffers used in protein purification are listed in Table 3.

Table 3 Recipes of buffers used in protein purification and growth assays. Buffer recipes for protein purification were obtained from the Blower Lab.

Buffer	Recipe
A500	20 mM tris-HCl, pH 7.9, 500 mM NaCl, 5 mM imidazole, and 10 % glycerol (v/v)
A100	20 mM tris-HCl, pH 7.9, 100 mM NaCl, 5 mM imidazole, and 10 % glycerol (v/v)
B100	20 mM tris-HCl, pH 7.9, 100 mM NaCl, 250 mM imidazole, and 10 % glycerol (v/v)
B100 2X imidazole	20 mM tris-HCl, pH 7.9, 100 mM NaCl, 500 mM imidazole, and 10 % glycerol (v/v)
C1000	20 mM tris-HCl, pH 7.9, 1000 mM NaCl, and 10 % glycerol (v/v)
1X PBS	137 mM NaCl, 2.7 mM KCl, 10 mM Na_2HPO_4, and 1.8 mM KH_2PO_4

The protein-containing fractions were pooled and incubated with hSENP2 SUMO protease, obtained from Blower lab at Durham University, overnight at 4 ^{o}C with gentle shaking to cleave the His_6-SUMO tag. To further concentrate and purify AdcAI from the His_6-SUMO tag, it was diluted to a final NaCl concentration of 30 mM with 20 mM tris-HCl pH 7.9 buffer and the pH was lowered to 6.5 by adding solid 3-(*N*-morpholino)propanesulfonic (MOPS) acid. Diluted protein sample was loaded onto HiTrap™ SP HP 5 mL column (Cytiva), washed with 10 CV of 20 mM tris-HCl pH 6.5 MOPS, and eluted with buffer A500.

To purify AdcAII from the His_6-SUMO tag, it was loaded onto a HisTrap™ HP 5 mL column, washed with 10 CV of buffer A500 and eluted with 5 CV of buffer B100. To remove any excess Ni ions, imidazole and Zn bound to the proteins, the protein-containing fractions were incubated with 100 mM ethylenediaminetetraacetic acid (EDTA) for 5 minutes and desalted using a PD-10 column by eluting with 50 mM MOPS buffer pH 7.4. At the end of the purification steps, we were able to obtain *apo*-AdcAI, but AdcAII still had Zn bound as the Zn binding site is buried in the protein.

2.2 Synthesis and handling of Hst5 peptides

The Hst5 peptides were synthesised commercially as the acetate salt and purified to >95 % (GenScript) and confirmed to be metal-free by ICP MS. Concentrations of stock peptide solutions

were determined using solution absorbances at 280 nm in 50 mM MOPS buffer pH 7.4 (ε_{280} = 2667 cm^{-1})

2.3 Chemical basis of metal reporting probes

The metal-binding affinities of the proteins were measured by competition assays using colourimetric and fluorometric indicators (probes) that bind metal and report the metal binding by changes in optical properties (absorbance, or fluorescence). In the case of colourimetric probes, the metalated and non-metalated forms typically absorb at different wavelengths, enabling visualisation and quantification of metal binding. In the case of fluorometric probes, metal-binding either lead to an increase or decrease of probe fluorescence.

For example, 4-(2-pyridylazo)resorcinol (PAR) has benzene rings which are involved in the metal binding, as shown in Figure 8. The *apo*-PAR absorbs at 420 nm due to the delocalised π electrons in the aromatic rings. Metal binding to *apo*-PAR induces a shift in absorbance to higher wavelengths (typically around 500 nm, depending on the metal) as a result of charge transfer.

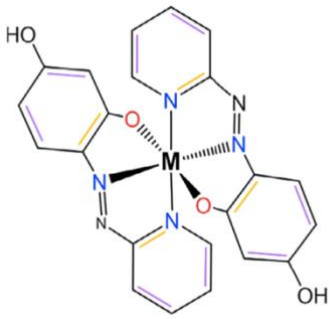

Figure 8 $Zn(PAR)_2$ complex. Zn stated as M.

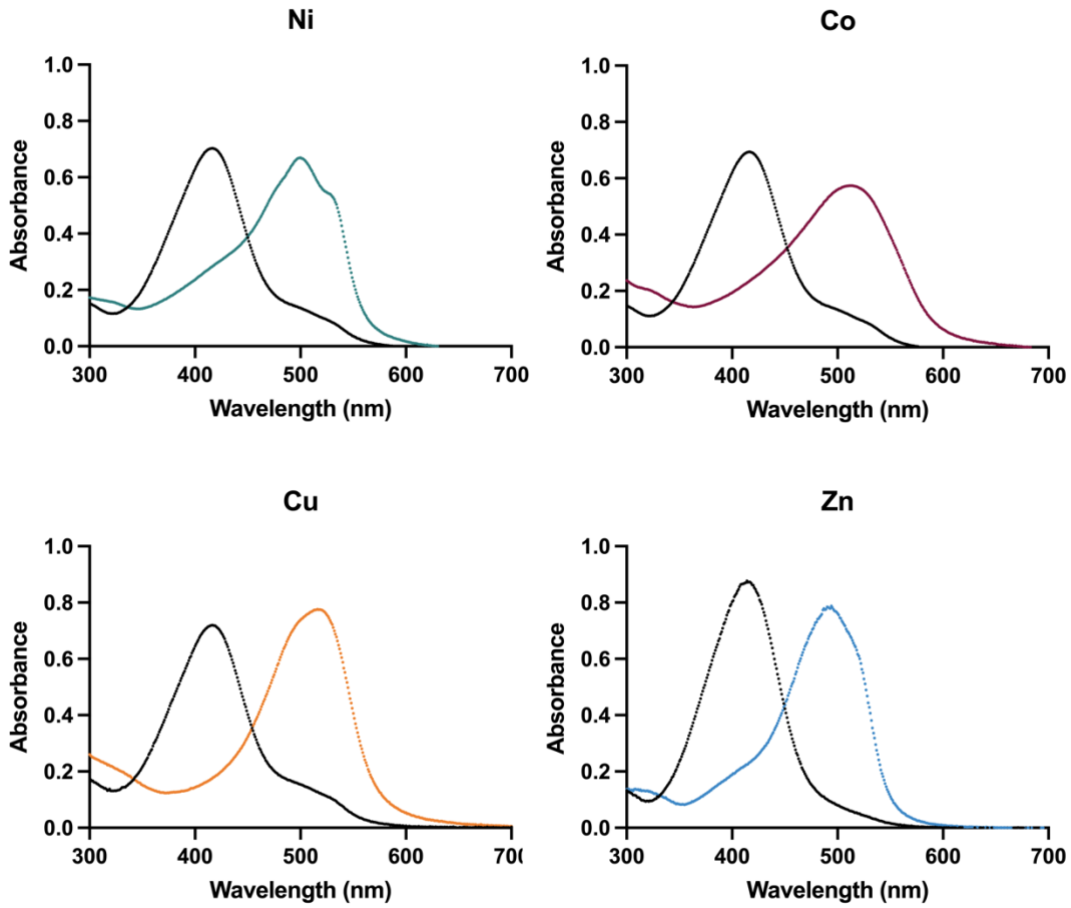

Figure 9 Spectral change of PAR in 6 M guanidine chloride 50 mM MOPS buffer pH 7.4. The peak absorbance of CoPAR is 512 nm, NiPAR 498 nm, CuPAR is 512 nm, and $Zn(PAR)_2$ is 495 nm.

More importantly, these probes bind metals with known dissociation constants ($K_D = 1/K_A$). The K_D of the known colourimetric probes used in this study is listed in Table 4. By using mass balance equations, the affinity of the unknown protein/ligand can be calculated.

2. Materials and Methods

The equilibrium of the competition assay can be expressed as:

$$P + ML \rightleftharpoons MP + L$$

or

$$P + ML_2 \rightleftharpoons MP + 2L$$

Where P = Protein, M = Metal, L = Ligand/Probe

The exchange constant (K_{ex}) for the above equilibrium can be expressed as:

$$K_{ex1} = \frac{[MP][L]}{[P][ML]}$$

or

$$K_{ex2} = \frac{[MP][L]^2}{[P][ML_2]}$$

The K_{ex} for each reaction can be rearranged with K_D(ML) and K_A(MP) as:

$$K_{ex1} = K_D(ML) \times K_A(MP)$$

$$= \frac{[M][L]}{[ML]} \times \frac{[MP]}{[M][P]}$$

$$= \frac{[MP][L]}{[P][ML]}$$

or

$$K_{ex2} = K_D(ML_2) \times K_A(MP)$$

$$= \frac{[M][L]^2}{[ML_2]} \times \frac{[MP]}{[M][P]}$$

$$= \frac{[MP][L]^2}{[P][ML_2]}$$

From the competition assay, K_{ex} can be calculated as the colourimetric probes report [ML] or [ML_2].

$[L]=[L]_{total}-[ML]$

$[MP]=[M]_{total}-[ML]$

$[P]=[P]_{total}-[MP]$

or

$[L]=[L]_{total}-[ML_2]$

$[MP]=[M]_{total}-[ML_2]$

$[P]=[P]_{total}-[MP]$

Therefore, the $K_A(MP)$ can be calculated using the K_{ex} equation rearranged:

$K_A(MP)=K_{ex}/K_D(ML)$

or

$K_A(MP)=K_{ex}/K_D(ML_2)$

By measuring the solution absorbance or fluorescence of a mixture of protein, probe, and metal, the total and the equilibrium concentrations of each of the components of the reaction can be determined. If K_A of the probe is known, then K_A (or K_D) of the protein can be calculated accordingly. These calculations were performed using DynaFit (Biokin Ltd).

2.3 Characterisation and calibration of stock solutions

2.3.1 Metal and probe stock calibration and competition assays

To calibrate the $CuCl_2$ stock solution, a master stock was prepared in 50 mM MOPS buffer pH 7.4 to contain a final concentration of 300 µM bicinchoninic acid (BCA) and 2000 µM ascorbic acid. Serial dilutions of $CuCl_2$ were prepared separately in deionised water. 900 µL of the master stock and 100 µL of the appropriate $CuCl_2$ stock was added to a cuvette. After 5 minutes of incubation at room temperature, solution absorbances were measured to determine the concentrations of $[Cu^{I}(BCA)_2]^{3-}$ complex. Absorbance at 562 nm (ε_{562} = 7900 $M^{-1}\,cm^{-1}$) was plotted against the Cu concentrations and the concentration of the $CuCl_2$ stock was calculated using the Beer-Lambert law (eq. 2).

$$2\ BCA + Cu(I) \rightleftharpoons [Cu^{I}(BCA)_2]^{3-} \qquad \text{(eq. 1)}$$

$$A = \varepsilon l c \qquad \text{(eq. 2)}$$

The calibrated stock of $CuCl_2$ was used to standardise the probes, which in turn were used to standardise the $ZnCl_2$ stock solution. Master stocks of probes were prepared in 50 mM MOPS buffer pH 7.4 and 135 µL of the master stock was aliquoted into an Eppendorf UVette. Serial dilutions of the calibrated $CuCl_2$ were newly prepared in deionised water and 15 µL of the appropriate dilution was added to the Eppendorf UVettes. Solution absorbances were measured from 300 nm to 800 nm and the peak absorbance of *apo*- and *holo*-probes were plotted against the metal concentration. The endpoints of the saturated probes were determined to calculate the concentrations of the probe stocks. The $ZnCl_2$ stock was calibrated with the same method. Although this method does not calculate the

absolute concentration of each probe stock solution, it relies on the concentration of $CuCl_2$, which is calibrated using $[Cu^{I}(BCA)_2]^{3-}$ with known extinction coefficient at 562 nm (ε_{562}).

Competitions assays were performed by preparing a master stock of the appropriate probe and the competing ligand in 50 mM MOPS buffer pH 7.4. Serial dilutions of the metal were prepared in deionised water separately. The master stock solution was aliquoted in 135 µL into Eppendorf UVettes and 15 µL of the diluted metal stocks were added to the stock solution to a desired final concentration. After incubating the mixture for 5 minutes at room temperature, solution absorbances were measured from 300 nm to 800 nm. The peak absorbance of *apo*- and *holo*-probes were plotted against the metal concentration. The plotted data was fitted in Dynafit using equilibrium models described in the script (Supplementary material 2 and 3). The K_D of all known probes used in the experiments are listed in Table 4.

Table 4 List of fluorometric and colourimetric metal indicators used in this study.

Name	K_D (M)	$\lambda_{max\ -apo}$	$\lambda_{max\ -holo}$	Reference
Zinc (II) indicators				
Zincon	1.26×10^{-5}	470 nm	620 nm	[84]
MagFura2	2.0×10^{-8}	373 nm	323 nm, 338 nm	[85]
Quin2	3.7×10^{-12}	262 nm	247 nm	[86]
FluoZin3	1.5×10^{-8}	-	*F*	[87]
PAR	9.1×10^{-13} *	420 nm	500 nm	[88]
Copper (I) Indicators				
BCA	6.25×10^{-18} M^2 *	N/A	562 nm (ϵ=7900 cm^{-1} M^{-1})	[89]
Copper (II) Indicators				
Zincon	1.75×10^{-16}	470 nm	607 nm	**
FluoZin3	9.1×10^{-11}	-	-	[90]
EDTA	1.26×10^{-16}	N/A	N/A	[91]
NTA	1.99×10^{-11}	N/A	800 nm	[92]
PAR	1.85×10^{-13}	420 nm	512 nm	**

F fluorescence, λ_{ex} = 494 nm, λ_{em} = 518 nm

* Refers to $1/\beta_2$ (M^2)

$\beta_2 = K_{A1} \times K_{A2}$ for two binding events as the metal-ligand binds 1:2

** Obtained from experiments in this study

2.3.2. Determination of AdcAI concentration

The protein properties of AdcAI were predicted using the ExPASy ProtParam tool giving a predicted extinction coefficient (ε) of 83200 $M^{-1}cm^{-1}$ at 280 nm. To measure the precise concentration of AdcAI stock solution, a master stock solution of Zincon and AdcAI was prepared in 50 mM MOPS buffer pH 7.4. 135 µL of the master stock was added with 15 µL of the serial dilutions of $ZnCl_2$ in Eppendorf UVettes. The peak absorbance of *apo*- and *holo*-Zincon was plotted against the concentration of $ZnCl_2$. As Zincon has a relatively weak affinity to Zn ($K_D = 1.26 \times 10^{-5}$ M), the absorbance of *holo*-Zincon only increases once AdcAI is fully saturated. The plotted data was used to calculate the starting point of *holo*-Zincon formation which is the concentration of Zn bound to AdcAI. The concentration of AdcAI was calculated by the stoichiometry of Zn-AdcAI (eq. 3).

$$2\ Zn(II) + AdcAI \rightleftharpoons Zn_2AdcAI \qquad \text{(eq. 3)}$$

From the calibrated AdcAI, the ε_{280} of AdcAI was calculated to be 58385 $M^{-1}cm^{-1}$. This value was used to calculate the concentration of AdcAI in further experiments.

2.4 Metal binding to proteins

2.4.1 Desalting columns to determine Hst5 Zn affinity range

To determine the approximate affinity of Hst5 to Zn, Hst5 (100 µM) and $ZnCl_2$ (150 µM) was incubated in 50 mM MOPS buffer pH 7.4 for 10 minutes at room temperature with a final volume of 500 µL. The mixture was passed through a Thermo Scientific™ Pierce™ Polyacrylamide Desalting column, 1.8 K MWCO, 5 mL, according to the manufacturer's protocol with 50 mM MOPS buffer. The eluted sample was collected in 500 µL fractions. Each fraction was validated for metal concentration and protein concentration.

Metal concentration was assessed in 50 mM MOPS buffer pH 7.4 with PAR by adding 6 M guanidine chloride to denature Hst5. A standard curve of PAR with $ZnCl_2$ was generated in 6 M guanidine chloride 50 mM MOPS buffer pH 7.4, and the peak absorbance of *holo*-PAR at 500 nm was plotted against the concentration of Zn. The absorbances of the column fractions were interpolated from the standard curve. The protein concentrations of the fractions were determined using the QuantiPro™ BCA Assay kit, following the manufacturer's protocol, but increasing the protein concentration of the fractions by 2-fold. The Zn concentration and protein concentration in each fraction was plotted against the volume eluted from the polyacrylamide column.

2.4.2 Binding of other metals to AdcAI

Apo-AdcAI (100 µM) was incubated with different metal salt solutions, $CoCl_2$, $MnSO_4$, $FeSO_4$, $NiSO_4$ and $CuCl_2$ (150 µM) in 50 mM MOPS buffer pH 7.4 for 10 minutes at room temperature with a final volume of 1000 µL. The mixtures were passed through a PD-10 column individually, which was equilibrated with 25 mL of 50 mM MOPS buffer pH 7.4 before loading the protein mixture. After the sample had gone into the column bed, the protein was eluted in 500 µL fractions by washing with 50

mM MOPS buffer pH 7.4. The peak fraction containing AdcAI was measured for A280 with a nanodrop to calculate the protein concentration using $\varepsilon_{280} = 58385\ M^{-1}\,cm^{-1}$. The protein fraction was added into 6 M guanidine chloride 50 mM MOPS buffer pH 7.4 to a final concentration of 5 µM, with 30 µM PAR or MF2 to a final volume of 150 µL. The solution absorbance was measured in an Eppendorf UVette from 300 nm to 800 nm which was plotted with a control sample of 30 µM PAR or MF2 in 6 M guanidine chloride 50 mM MOPS buffer pH 7.4, not containing AdcAI. The peak absorbance of the samples that had a shift in solution absorbance were interpolated with a standard curve generated with each metal in 30 µM PAR in the same buffer, to calculate the concentration of metal bound to 5 µM AdcAI. The desalting experiment with a PD-10 column was repeated with $ZnCl_2$, $CuCl_2$ and an equal mixture of both $ZnCl_2$ and $CuCl_2$ and the peak fraction was sent for ICP MS.

2.5 Growth and manipulation of *S. pyogenes*

2.5.1 Culture conditions

Glycerol stocks stored at -80 °C were propagated onto solid Todd Hewitt medium (THY) containing 0.2 % yeast extract and incubated at 37° C overnight. Colonies were harvested and resuspended in 1X phosphate-buffer saline (1X PBS), which was inoculated in liquid cultures of a chemically defined medium containing glucose as carbon source (CDM-glucose, recipe from Stewart et al., 2020) [93]. Both solid and liquid growth media contained 50 µg/mL catalase.

2.5.2 Growth assays

Colonies from an overnight growth on THY agar were resuspended in 1X PBS and inoculated in CDM-glucose to an $OD_{600} = 0.01$. Growth was monitored at 37 °C in flat-bottomed 96-well plates with 200 µL per well. Zn was added at 0, 2, 5, 10 µM in each well in both *S. pyogenes* WT and △*czcD* and Cu was added at 0, 5, 10, 20 µM in *S. pyogenes* WT and △*copA*. 50 µM of filter sterilised Hst5 was added to wells containing Hst5. The 96-well plates were sealed with gas permeable, optically clear membrane (Diversified Biotech). OD_{600} values were read every 20 minutes for 10 hours, shaken immediately before each reading (200 rpm, 1 min, double orbital mode). OD_{600} values were not corrected for path length (*ca.* 0.58 cm for a 200 µL culture).

Table 5 Bacterial strains used in this study

Bacterial strains	**Description**	**Origin/Reference**
Streptococcus pyogenes		
5448	*S. pyogenes* invasive M1T1 strain	[94]
5448Δ*copA*	*S. pyogenes* 5448 *copA*::*kan* deletion mutant	[93]
5448Δ*czcD*	*S. pyogenes* 5448 *czcD*::*spc* deletion mutant	[95]
Escherichia coli		
DH5α	Cloning host DH5α (from Blower Lab)	Blower lab (Durham University)
BL21(DE3) Rosetta 2	Expression host with rare codons Cm30 Resistance	Lab collection

3. Results

3.1 Metal affinities of Colourimetric probes

3.1.1 PAR Cu binding affinity

Before determining affinities of AdcAI and Hst5, probes of unknown affinity to Cu were determined to be used for competition assays for measuring Cu affinity.

$$PAR + Cu^{II}NTA \rightleftharpoons Cu^{II}PAR + NTA \qquad \text{(eq. 4)}$$

(420 nm) (512 nm) λ_{max}

In PAR, the spectral absorbance at 420 nm due to *apo*-PAR decreases and the absorbance at 512 nm due to Cu-PAR increases in a linear fashion upon Cu titration (Figure 10B and C). A clear isosbestic point can be observed in the spectra (Figure 10A), indicating direct conversion of *apo*-PAR to Cu-PAR without formation of additional species. An end point at 20 µM Cu was observed when 20 µM PAR was used, consistent with a 1:1 stoichiometry.

To obtain the binding affinity of Cu to PAR, this probe was competed with NTA, whose binding affinity is known (K_D = 1.99 × 10^{-11} M). Compared to the direct addition of Cu into PAR, the Cu-dependent spectral changes were more gradual in the presence of NTA (Figure 10C and D). A clear isosbestic point was also observed (Figure 10B), again indicating the formation of only the 4 species in Equation 4 without forming any ternary complexes. The data were fitted to an equilibrium model in Dynafit giving Cu-PAR K_D = 1.85 × 10^{-13} M. Curve fits using affinities that were ten times weaker (K_D = 1.85 × 10^{-12} M) and 10 times tighter (K_D = 1.85 × 10^{-14} M) were simulated. The weaker simulated fit clearly departed from the experimental data points for the competition between NTA and PAR (Figure 10C and D). The tighter simulated fit resembled the experimental data points for the direct titration of Cu into PAR in the absence of NTA (Figure 10 C and D). Therefore, both simulations gave confidence that the K_D value obtained for PAR was in the correct range.

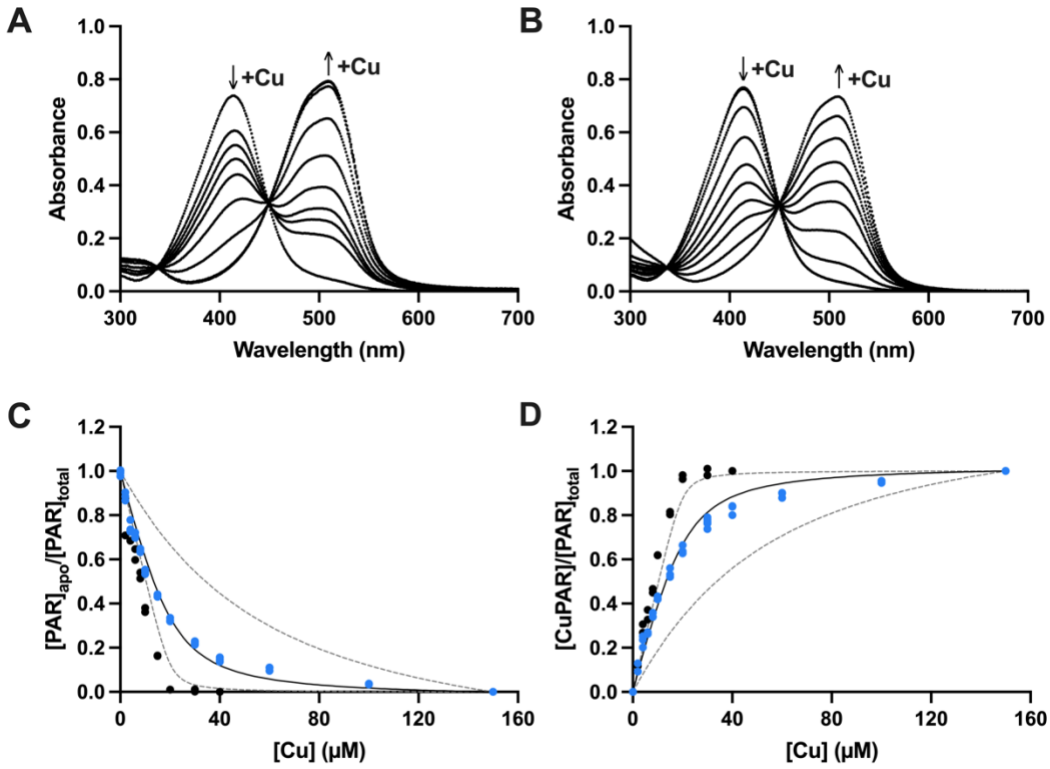

Figure 10 A Spectral change upon addition of Cu into PAR. The maximum absorbance of *apo*-PAR at 420 nm decreases and Cu-PAR at 512 nm increases. **B** Spectral change upon addition of Cu in PAR in the presence of NTA. The maximum absorbance of *apo*- and Cu-PAR is the same as PAR alone. **C** Normalised plot of the changes in solution absorbance of *apo*-PAR at 420 nm and **D** Cu-PAR at 512 nm upon addition of Cu in the absence (black) or presence (blue) of 400 μM NTA in 20 μM PAR. The solid black line showing the model fit to the data and dashed lines showing the 10-fold stronger and weaker fit of the model (Cu-PAR K_D = 1.85 × 10^{-13} M). All experiments were performed in 50 mM MOPS buffer pH 7.4.

3.1.2 Zincon Cu binding affinity

In Zincon, the spectral absorbance at 470 nm due to *apo*-Zincon decreases and the absorbance at 607 nm due to Cu-Zincon increases in a linear fashion upon Cu titration (Figure 11C). A clear isosbestic point can be observed in the spectra (Figure 11A), indicating direct conversion of *apo*-Zincon to Cu-Zincon without formation of additional species. Consistent with the expected 1:1 stoichiometry, an endpoint at 10 μM Cu was observed when 10 μM Zincon was used.

The dissociation constant of Zincon-Cu is known to be 4.68 × 10^{-17} M from previous studies [96]. To varify the binding affinity of Cu to Zincon, this probe was competed with EDTA, whose binding affinity

is known (K_D = 1.26 × 10^{-16} M). Compared to the direct addition of Cu into Zincon, the Cu-dependent spectral changes were more gradual in the presence of EDTA (Figure 11C). A clear isosbestic point was also observed (Figure 11B), again indicating the formation of only the 4 species in Equation 5 without forming any ternary complexes. The data were fitted to an equilibrium model in Dynafit giving Cu-Zincon K_D = 1.75 × 10^{-16} M. The reassessed affinity of Cu-Zincon is within a similar range with the previously measured data, therefore confirming both the literature and the measurements from this study. The fit shows a sharp endpoint rather than a curve as both the affinities of EDTA and Zincon to Cu(II) are approximately 10 orders of magnitude higher than the concentration of Cu and ligands used in the competition assay.

$$\text{Zincon} + \text{Cu}^{\text{II}}\text{EDTA} \rightleftharpoons \text{Cu}^{\text{II}}\text{Zincon} \qquad \text{(eq. 5)}$$

$$\text{(470 nm)} \qquad \text{(607 nm)} \qquad \lambda_{max}$$

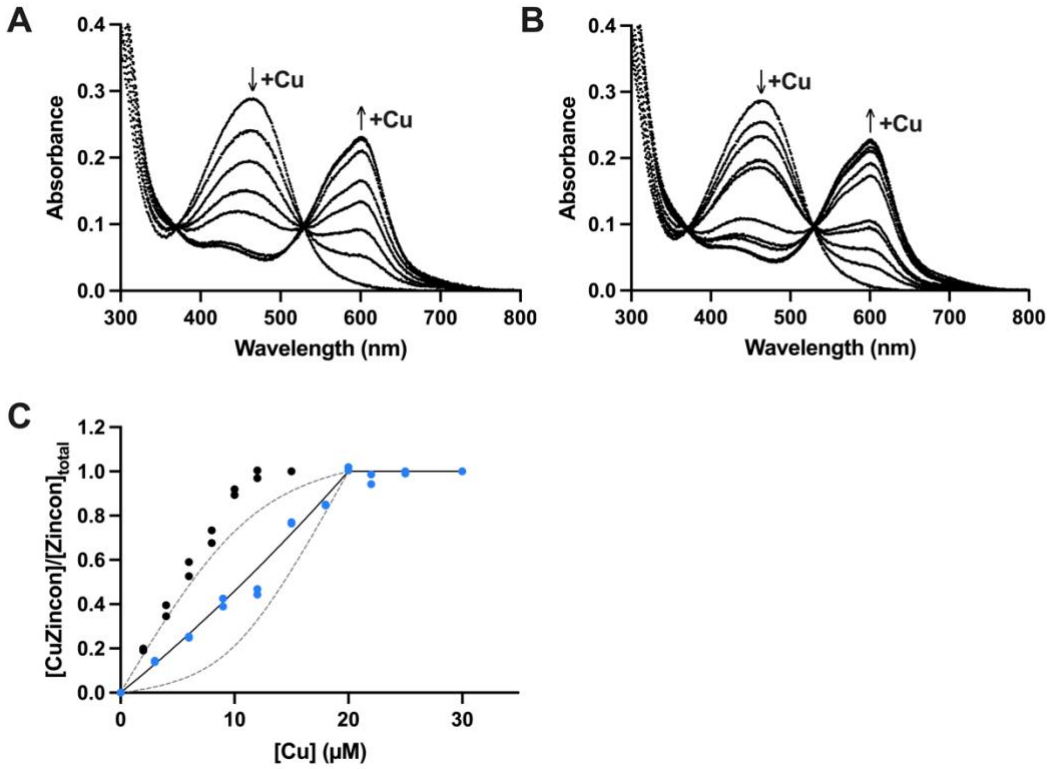

Figure 11 A Spectral change upon addition of Cu in Zincon. The maximum absorbance of *apo*-Zincon at 470 nm decreases and Cu-Zincon at 607 nm increases. **B** Spectral change upon addition of Cu in Zincon in the presence of EDTA. The maximum absorbance of *apo*- and Cu-Zincon is the same as

Zincon alone. **C** Normalised plot of the changes in solution absorbance of Cu-Zincon at 607 nm upon addition of Cu in the absence (black) or presence (blue) of 10 μM EDTA in 10 μM Zincon. The solid black line showing the model fit to the data and dashed lines showing the 10-fold stronger and weaker fit of the model (Cu-Zincon K_D = 1.75 × 10^{-16} M).

3.2 Overexpression and purification of AdcAI and AdcAII

AdcAI and AdcAII were overexpressed and purified as recombinant proteins in *E. coli* to isolate the proteins for measuring metal binding affinities *in vitro*. Both genes were amplified by PCR using *S. pyogenes* M5005 as a template. Both proteins are surface-attached lipoproteins, so only the nucleotide sequences coding for the soluble domains were amplified, namely from the 21st and 30th amino acid in AdcAI and AdcAII respectively, following previously established methods. The PCR products were inserted into pSATL after a His_6-SUMO tag. This strategy enabled each protein to be expressed with an N-terminal tag for purification. The His_6-SUMO tag has 6 His residues, which binds tightly to the Ni column for easier purification. The His_6-SUMO tag was subsequently removed by cleavage using hSENP SUMO protease, which recognises the Gly-Gly cleavage motif, as shown in Figure 12. This strategy did not leave any residues that are not part of the original protein. The plasmids were then transferred into the expression host, *E. coli* BL21 Rosetta2 which is competent of expressing proteins with rare codons. The expression of proteins from GAS in *E. coli* requires the competent cell to carry the expression of rare codons because the codons are not the same so the expression host may lack the corresponding tRNA and result in stalled translation. The *E. coli* BL21 Rosetta2 carries chloramphenicol resistance, also for selection.

AdcAI and AdcAII were successfully subcloned into the *E. coli* host (Figure 13A) and subsequently purified (Figure 13B). Both proteins were purified with contaminating Ni and Zn from the culture media and/or the Ni column. Contamination by Ni or Zn was determined by denaturing the protein with 6 M guanidine chloride and checking for the presence of metal ions with PAR. The Ni-PAR and Zn-PAR complexes display distinct spectral features in the visible range (300 nm to 800 nm), which allow the metals to be identified. These metal ions were removed by adding 100 mM EDTA and desalting on a PD-10 gel filtration column. The desalted proteins were confirmed to be *apo*- by using the same method

using 6 M guanidine chloride and PAR. We were able to obtain *apo*-AdcAI, but AdcAII still had Zn bound (1:1 stoichiometry). Previous studies of AdcAII in *S. pneumoniae* suggest that the Zn binding site of AdcAII, which contains His66, His142, His206 and Glu281, is buried in the protein and that Zn is likely kinetically trapped in the protein by the flexible loop (Figure 6) [97]. Removal of this bound Zn required overnight dialysis with 10-50 mM EDTA at low pH buffer to protonate the imidazole His sidechains and weaken metal binding. Due to time constraints, the AdcAII protein was not pursued further in this study.

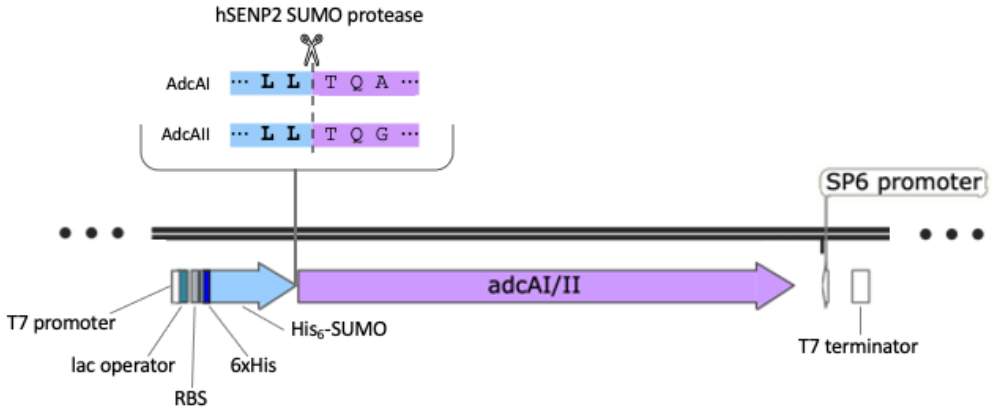

Figure 12 Overexpression constructs of *adcAI* and *adcAII* in pSATL. Target genes are inserted after the His_6-SUMO tag with the Gly-Gly recognition site for hSENP SUMO protease cleavage. Gene insert starts from 60th and 87th base pair in *adcAI* and *adcAII* accordingly, to exclude the transport signal.

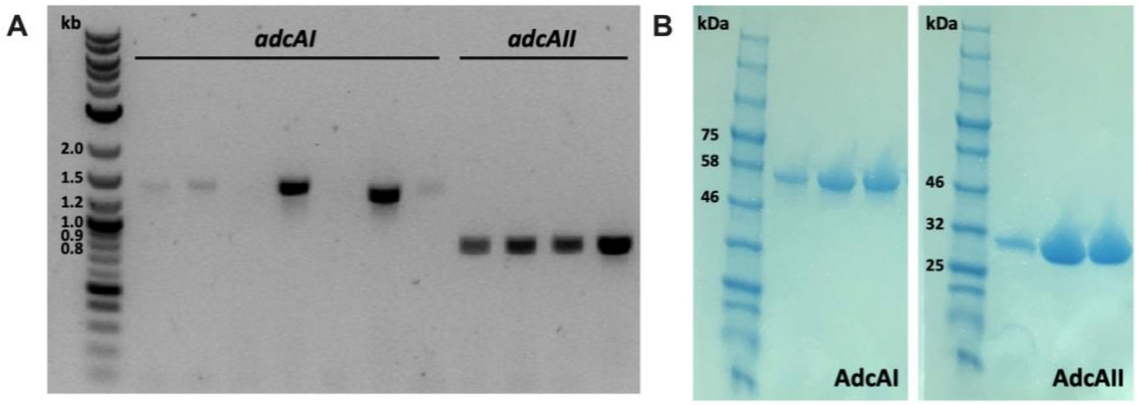

Figure 13 A Colony PCR of transformants *adcAI* (1489 bp) and *adcAII* (835 bp) to confirm successful transformation of the plasmid with gene inserts into *E. coli* DH5a. **B** Protein gel of AdcAI (56 kDa) and AdcAII (31 kDa) overexpression in *E. coli* BL21 Rosetta2, after cleavage of the His_6-SUMO tag.

3.3 Metal-binding profiles of AdcAI

Previous studies have shown that AdcAI has two Zn binding sites, the tighter N-terminal site and weaker C-terminal site [66]. Different metals were tested for binding to AdcAI to examine whether AdcAI can bind and import other metals via the AdcABC system. Previously, in *S. pneumoniae*, different metals were loaded on to the Zn binding sites of AdcAI to test for the stability of the protein. Whilst Mn, Fe, and Cu did not significantly affect the melting point of the protein, Co, Ni, and Zn loading appeared to stabilise the protein. The stability of the protein is achieved upon metal binding as metalation results in conformational change of the protein to enable the function of the protein, to transfer Zn to AdcB.

To determine whether the *S. pyogenes* AdcAI can bind metal other than Zn, 100 µM AdcAI was incubated with 150 µM Zn, Co, Ni, Cu, Fe, and Mn individually and desalted through a PD-10 desalting column to remove excess, unbound metals. Protein-containing fractions were denatured and tested for metal content in the protein using PAR as a colourimetric indicator for Zn, Co, Ni, Cu, and Fe and MF2 for Mn. The absorbance intensities at the relevant wavelengths were compared against a standard curve for the relevant metal. The results are summarised in Table 6.

AdcAI was confirmed to bind Zn in a 1:2 stoichiometry, which are likely to bind at the N-terminal and C-terminal Zn binding sites. The spectral changes show that Co, Ni, and Cu were bound to AdcAI while Fe and Mn were not (Figure 14). Such binding event may occur *in vivo* when the metal availability of Co, Ni, and Cu is high. However, this does not mean that they are imported via the AdcABC system as the import of metal may require a specific interaction of the protein and the bound metal to trigger correct conformational change for the metal to be transferred from AdcAI to AdcB. Further studies are required to investigate the import of these metals through the AdcABC system.

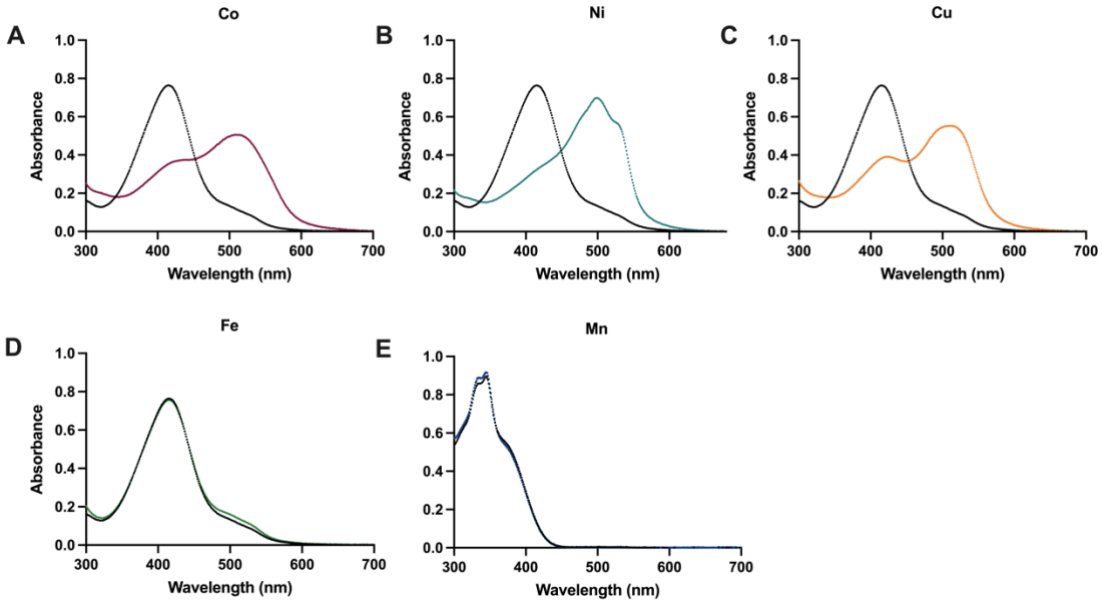

Figure 14 The spectral shift of 30 µM PAR (black, A-D) and 30 µM MF2 (black E) upon addition of 5 µM denatured AdcAI (coloured) shows the presence of metal bound to the protein after incubation with each metal and desalting.

Table 6 Concentration of metal present in 5 µM AdcAI derived from PAR standard curve in 50 mM MOPS pH 7.4, 6 M guanidine chloride.

Metal	Concentration (µM)	Metal:AdcAI ratio
Zn	-	2 : 1
Co	8.99	1.9 : 1
Ni	10.2	2.04 : 1
Cu	10.4	2.08 : 1

3.3.1 Cu(II) binding affinity of AdcAI

Given that AdcAI binds to Cu with a 1:2 stoichiometry, the affinity for Cu was assessed to understand Cu binding properties of AdcAI. First, Cu and Zn were directly competed for binding to AdcAI. As with most proteins, it was expected that the Cu affinity would be higher than Zn, since Cu sits at the top of the Irving-Williams series. AdcAI was incubated with an equal concentration of excess Cu and Zn, followed by desalting with a PD-10 desalting column. Fractions containing AdcAI were checked for metal content by ICP MS. The ICP MS analysis confirmed that AdcAI binds Cu or Zn with a 1:2 stoichiometry. In the Cu and Zn competition, the majority of the metal bound to AdcAI is Cu, but there

is also Zn present in the sample. This may imply that Zn binding in one binding site is outcompeted by Cu, but the other metal binding site binds them equally. However, the total metal content in this data exceeds the 1:2 ratio, so it would be worth repeating this experiment to determine the accuracy of the metal stoichiometry.

Table 7 ICP MS of AdcAI incubated Zn and/or Cu

	μM			
Sample	**AdcA**	**Cu**	**Zn**	**Metal:AdcA ratio**
AdcAI + Zn	33	1.0	67.6	1:2.05
AdcAI + Cu	33	64.3	0.5	1:1.95
AdcAI + Zn + Cu	33	49.8	27.0	1:1.5:0.8

As Cu binding to AdcAI seemed to be dominant over Zn binding, probes with affinities approximately in that range was used to determine Cu affinity of AdcAI. PAR (K_D = 1.85 × 10^{-13} M) was used to compete with AdcAI for Cu binding. *Apo*-PAR has peak absorbance at 420 nm which decreases upon addition of Cu. As Cu is added, a new peak appears at 512 nm, corresponding to the Cu-PAR species. 100 μM AdcAI was incubated with 150 μM Cu, desalted through the PD-10 desalting column to obtain Cu_2-AdcAI. To detect the strength of Cu bound to AdcAI, PAR was competed with Cu_2-AdcAI. The absorbance at 512 nm was monitored to track the formation of CuPAR complex with Cu_2-AdcAI added, and the peak absorbance at 512 nm was interpolated with a standard curve. PAR was able to capture 1.36 Cu from 1 AdcAI. This suggests that the weak Cu binding site of AdcAI has a lower affinity than PAR, thus outcompeted by PAR. Therefore, this competition sets the higher limit of the affinity at 1.85 × 10^{-13} M. Also, the tight Cu binding site of AdcAI competes with PAR resulting in partial chelation of Cu by PAR. However, although PAR would compete with AdcAI for the tighter Cu binding site, the spectra in Figure 15A suggest formation of ternary complexes of AdcAI, PAR and Cu. Therefore, PAR cannot be used to measure the affinity of Cu-AdcAI as the species formed in this equilibrium cannot be identified by the spectra.

For the tight Cu affinity of AdcAI, Zincon (K_D = 1.75 × 10^{-16} M) was used for a competition assay. *Apo*-Zincon has a peak absorbance at 470 nm which decreases upon addition of Cu and increasing peak

absorbance at 607 nm, corresponding to Cu-Zincon. A clear endpoint was observed when 10 µM Cu was added to 10 µM Zincon, consistent with the expected stoichiometry of 1:1 Cu:Zincon. The absorbance at 607 nm was monitored to track the formation of Cu-Zincon complex with (blue) and without (black) 5 µM AdcAI (Figure 15B). The AdcAI present in the equilibrium did not affect the Cu binding to Zincon suggesting that both metal binding sites of AdcAI are outcompeted by Zincon. Thus, this competition could only set the higher limit of the affinity of the tighter binding site at K_D = 1.75 × 10^{-16} M.

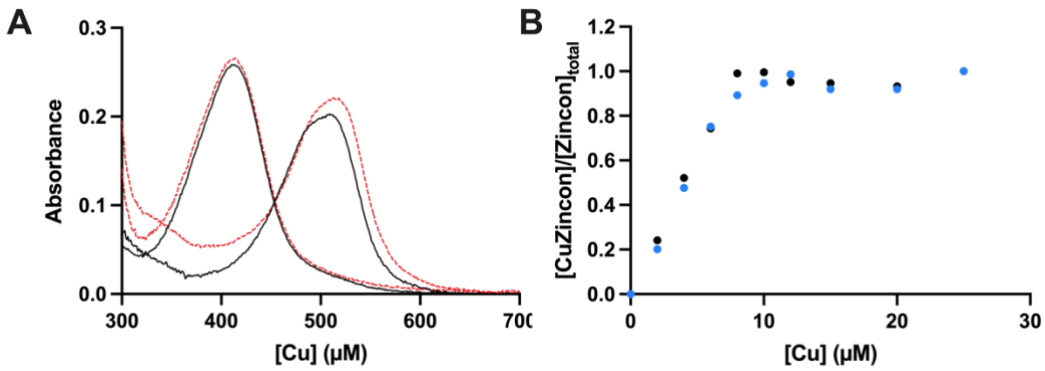

Figure 15 A Spectral change of PAR, in the presence (red) and absence (black) of AdcAI upon addition of Cu. The shape of the spectra shifts in the presence of AdcAI indicating tertiary structure formation. **B** Normalised plot of the changes in solution absorbance of Cu-Zincon at 607 nm upon addition of Cu in the absence (black) or presence (blue) of 5 µM AdcAI in 10 µM Zincon. AdcAI is outcompeted by Zincon.

Overall, the exact Cu(II) affinity of AdcAI was not determined. Nevertheless, the tighter Cu binding site in this protein is weaker than Zincon and similar to PAR. The weaker Cu binding site is weaker than PAR and similar or greater than the weaker Zn binding site. These approximate affinities show that Cu may bind to AdcAI even in the presence of Zn and could be imported into the cell if Cu binding triggers the correct mechanism of import. The affinities can be compared with metal chelating molecules such as Hst5 to predict whether those chelators will have an impact on intracellular Cu availability in *S. pyogenes*.

3.3.2 Affinity of the weak Zn-binding site of AdcAI

AdcAI has two Zn binding sites, the tighter site in the N-terminal domain and the weaker site in the C-terminal domain. Previously, the affinities have been measured by ITC. Here, the affinity of each binding sites for Zn were measured by competition with Zn binding probes.

First, MF2 (K_D = 2.0 × 10^{-18} M) was used to compete with the weak Zn binding site of AdcAI. *Apo*-MF2 has a peak absorbance at 372 nm which decreases upon addition of Zn. At the same time, two new peaks appear at 323 nm and 338 nm, corresponding to the Zn-MF2 species. A clear end point was observed when 10 µM Zn was added to 10 µM MF2, consistent with the expected stoichiometry of 1:1 Zn:MF2. The new absorbance at 372 nm was monitored in this study to track the formation of Zn-MF2 complex with (blue) and without (black) 5 µM AdcAI (Figure 16B). The competition curves show two distinguishable slopes, a near flat line from 0 to 5 µM and a gradient from 5 to 20 µM Zn added. In the first 5 µM Zn added, very little of the Zn-MF2 complex is formed, indicating that the Zn added is binding to AdcAI. This suggests that the tight Zn binding site of AdcAI has a higher affinity than MF2, thus outcompeting MF2. Therefore, this competition could only set the lower limit of the affinity at K_D = 2.0 × 10^{-8} M. In the next 15 µM of Zn added, competition between 10 µM MF2 and 5 µM of AdcAI was observed. An equilibrium model was fitted to the data on Dynafit giving the K_D of the weaker binding site of 6.7 × 10^{-8} M.

Zn^{II}☐		Zn^{II}		$Zn^{II}Zn^{II}$		☐	
AdcAI	+	MF2	⇌	AdcAI	+	MF2	(eq. 6)
		(323, 338 nm)				(372 nm)	λ_{max}

☐ = empty binding site on either protein or probe

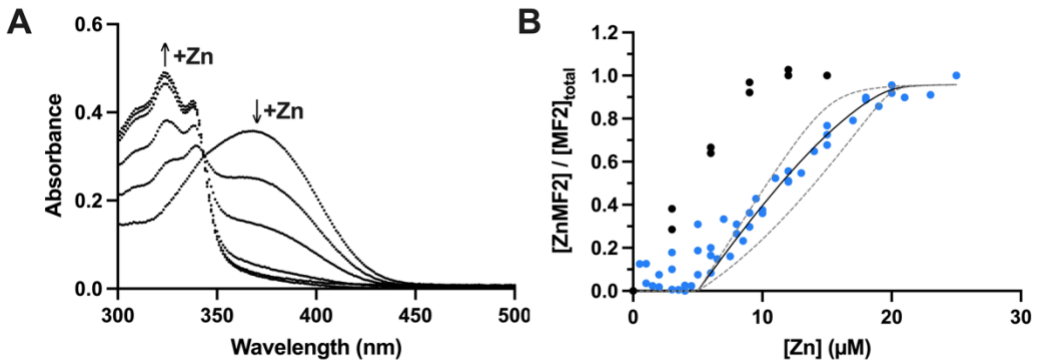

Figure 16 A Spectral change upon addition of Zn into MF2. The maximum absorbance of *apo*-MF2 at 372 nm decreases and Zn-MF2 at 323, 338 nm increases. **B** Normalised plot of the changes in solution absorbance of Zn-MF2 at 372 nm upon addition of Zn in the absence (black) or presence (blue) of 5 μM AdcAI in 10 μM MF2. The solid black line showing the model fit to the data and dashed lines showing 10-fold stronger and weaker fit of the model (Zn-AdcAI (weak site) K_D = 6.7 × 10^{-8} M).

3.3.3 Affinity of the tight Zn-binding site of AdcAI

Given that the tight Zn binding site has a higher affinity than MF2, Quin2 (K_D = 3.7 × 10^{-12} M) was used as the competitor. *Apo*-Quin2 has a peak absorbance at 262 nm which decreases upon addition of Zn. At the same time, a peak at 247 nm appears, corresponding to the Zn-Quin2 species. A clear endpoint was observed when 7 μM Zn was added to 7 μM Quin2, consistent with the expected stoichiometry of 1:1 Zn:Quin2. The new absorbance at 262 nm was monitored to track the formation of Zn-Quin2 complex with (blue) and without (black) 10 μM AdcAI (Figure 17B). This absorbance overlaps partially with the absorbance of the *apo*-protein AdcAI (λ_{max} = 280 nm), so the absorbance of the AdcAI was subtracted from the Zn-Quin2 absorbance to obtain the normalised spectra. The competition curve shows a more gradual decrease of *apo*-Quin2 compared to the direct addition of Zn into Quin2. An equilibrium model was fitted to the data on Dynafit giving the K_D of the tighter binding site of 5.3 × 10^{-13} M. The fit to data is poor at high Zn concentrations that saturated the probe (above 17 μM) because the absorbance readings were noisy. Nevertheless, the model employed yielded the best fit to the data and allowed us to estimate the affinity of the tight site. Affinities measured of both sites confirmed that there are two distinct Zn binding sites of two different affinities, with approximately 10000-fold difference between the two sites. These values are much tighter than the values from literature which were measured by ITC.

$$\underset{\square\square}{\text{AdcAI}} + \underset{\text{(247 nm)}}{\text{Quin2}} \rightleftharpoons \underset{\text{Zn}^{II}\square}{\text{AdcAI}} + \underset{\text{(262 nm)}}{\text{Quin2}} \qquad \text{(eq. 7)}$$

λ_{max}

$\square$ = empty binding site on either protein or probe

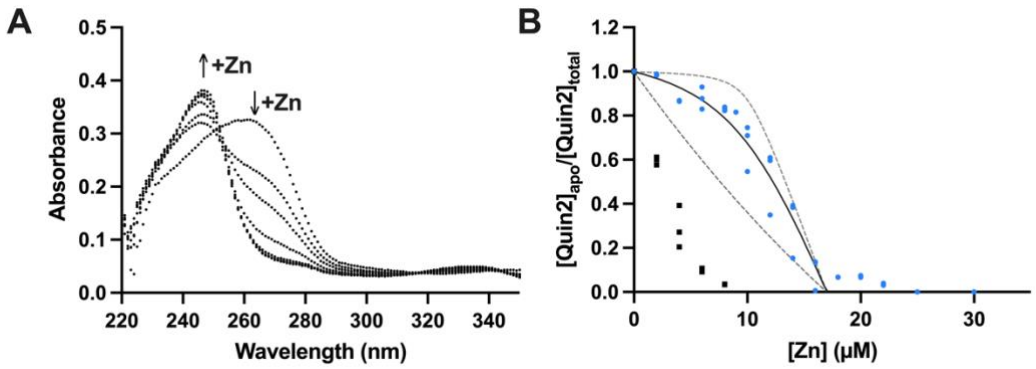

Figure 17 A Spectral change upon addition of Zn into Quin2. The maximum absorbance of *apo*-Quin2 at 262 nm decreases and Zn-Quin2 at 247 nm increases. **B** Normalised plot of the changes in solution absorbance of Zn-Quin2 at 262 nm upon addition of Zn in the absence (black) or presence (blue) of 10 μM AdcAI in 7 μM Quin2. The solid black line showing the model fit to the data and dashed lines showing the 10-fold stronger and weaker fit of the model (Zn-AdcAI (tight site) K_D = 5.3 × 10^{-13} M). One set of data was repeated by Dr Karrera Djoko.

3.4 Hst5 binds Zn with less than micromolar affinity

We next wished to investigate whether Hst5 can outcompete AdcAI for binding Zn and therefore prevent Zn from being imported into the cell and confer nutritional immunity. Previous literature showed that the Zn affinity of Hst5 is K_D = 1 × 10^{-5} M by ITC [51]. To confirm this weak binding, 100 μM Hst5 and 150 μM Zn were incubated together and eluted through a polyacrylamide column. Each fraction was

analysed for peptide content and metal content. The results showed that Zn did not co-elute with Hst5, suggesting that the Zn-Hst5 complex dissociated during passage through the column (Figure 18A). This result is consistent with the predicted weak micromolar affinity of Hst5 to Zn and indicates that this peptide should not compete with AdcAI.

To further confirm that Hst5 will be outcompeted by AdcAI for binding Zn, Hst5 was competed with MF2. The results showed that Hst5 was outcompeted by MF2 (Figure 18B). Under the same conditions, the weaker C-terminal Zn binding site of AdcAI was able to compete with MF2 (Figure 16B). Therefore, Hst5 has an Zn affinity that was lower than the weaker Zn binding site of AdcAI. Hst5 will not be able to chelate Zn from the Zn import system and thus it is not likely to exert a nutritional immunity effect.

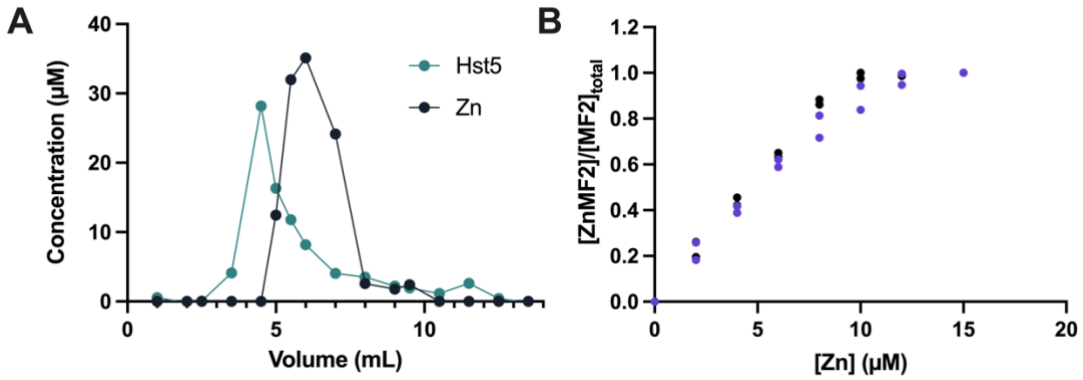

Figure 18 A Separation of HST and Zn through a polyacrylamide desalting column. **B** Normalised plot of the changes in solution absorbance of Zn-MF2 at 338 nm upon addition of Zn in the absence (black) or presence (purple) of 10 μM Hst5 in 10 μM MF2. Hst5 is outcompeted by MF2.

3.5 Hst5 binds Cu(II) with pM affinity

Although Cu is not required as a nutrient in *S. pyogenes*, the affinity of Hst5 to Cu was measured to predict the impact of Hst5 on *S. pyogenes* and for further studies in oral pathogens that require Cu in growth and pathogenicity. Previously, the Cu affinity of Hst5 was measured by competition assays with NTA, which generated $K_D = 7.9 \times 10^{-12}$ [52]. This competition was repeated in this study.

The spectral absorbance at 800 nm due to *holo*-NTA increases in a linear fashion upon Cu titration (Figure 19C). As *apo*-NTA does not absorb the visible range, the titration spectra do not form an isosbestic point. Similarly, the spectral absorbance at 530 nm due to Cu-Hst5 increases in a linear fashion upon Cu titration (not shown in data). Both absorbances were used to fit an equilibrium model to obtain K_D = 2.3 × 10^{-11} M, which is similar to the previously established value. However, NTA is not an ideal probe for measuring Cu affinity because the absorbance at 800 nm does not reach an endpoint even when the probe is fully saturated at 1:1 stoichiometry (Figure 19C). This is likely due to the formation of ternary structure complexes with the buffer, which is also indicated by the change in the spectral shape in Figure 19A. Similarly, we did not observe a clear end point at 530 nm due to the formation of other species which may involve a complex with the buffer or multiple binding of Cu to Hst5.

$$Cu^{II}NTA + Hst5 \rightleftharpoons Cu^{II}Hst5 + NTA \qquad \text{(eq. 8)}$$

(800 nm) (530 nm) λ_{max}

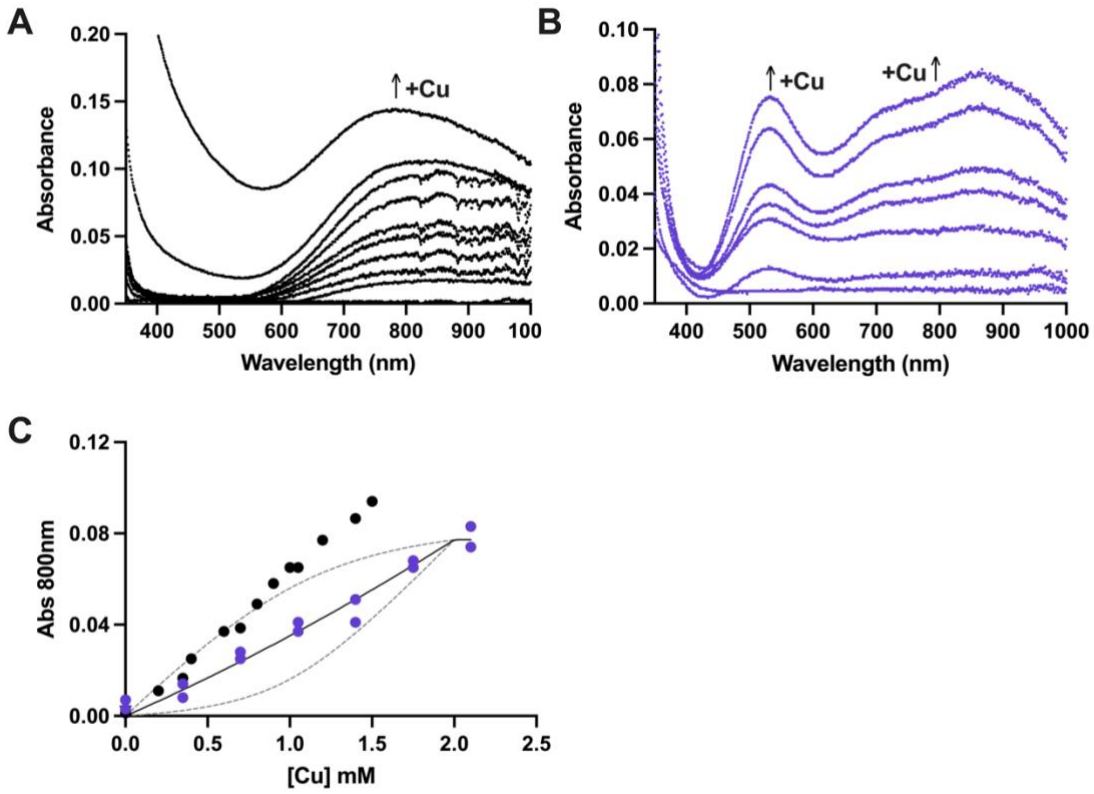

Figure 19 A Spectral change upon addition of Cu into NTA. The maximum absorbance of Cu-NTA at 800 nm increases. **B** Spectral change upon addition of Cu in NTA and Hst5. The maximum absorbance of Cu-NTA at 800 nm increases and Cu-Hst5 at 530 nm. **C** Normalised plot of the changes in solution absorbance of Cu-NTA at 800 nm upon addition of Cu in the absence (black) or presence (purple) of 1 mM Hst5 in 1 mM NTA. The solid black line is the model fit to the data and dashed lines are the 10-fold stronger and weaker fit of the model (Cu-Hst5 K_D = 2.39 × 10^{-11} M).

To improve our estimate of the Cu(II) binding affinity of Hst5, the next probe used was FluoZin3 (FZ3) (K_D = 9.1 × 10^{-11} M). Previously, Cu affinity of FZ3 has been determined by competing with Zn, observed by the quenching of fluorescence as Cu is added into the mixture of Zn-FZ3 (black in Figure 20A) [90]. As the affinity of FZ3 to Zn is K_D = 1.5 × 10^{-8} M, we do not expect that Hst5 (K_D = 1 × 10^{-5} M) would compete with FZ3 for Zn binding. This allowed us to compete FZ3 and Hst5 for Cu binding.

In the experiment, Cu was added to an equal concentration of FZ3 and Hst5 at 400 nM each, with slight excess of Zn at 500 nM. Addition of Cu replaces the Zn bound to FZ3, quenching the fluorescence. The Hst5 present in the sample also binds Cu, reducing the Cu binding to FZ3. The competition between Hst5 and FZ3 suppresses the fluorescence quenching. The fluorescence data were fitted to the

equilibrium model in equation 9, using the affinity of Zn-Hst5 (K_D = 8.3 × 10^{-6} M) measured by Isabel Holmes in the lab (Figure 20A). However, the model did not fit the data at higher Cu points. A new model was fit with the assumption that the Cu-FZ3 affinity is 10-fold lower than the published value (Figure 20B). As the initial model using Cu-FZ3 K_D = 9.1 × 10^{-11} M did not fit the data, the affinity of Cu-Hst5 measured by competition with FZ3 cannot be accurate. However, as the new model fit the data, it is worth evaluating the affinity of Cu-FZ3 for future use.

$$Zn^{II}FZ3 + Cu^{II}Hst5 \rightleftharpoons Cu^{II}FZ3 + Zn^{II}Hst5 \qquad \text{(eq. 9)}$$

(Fluorescence)

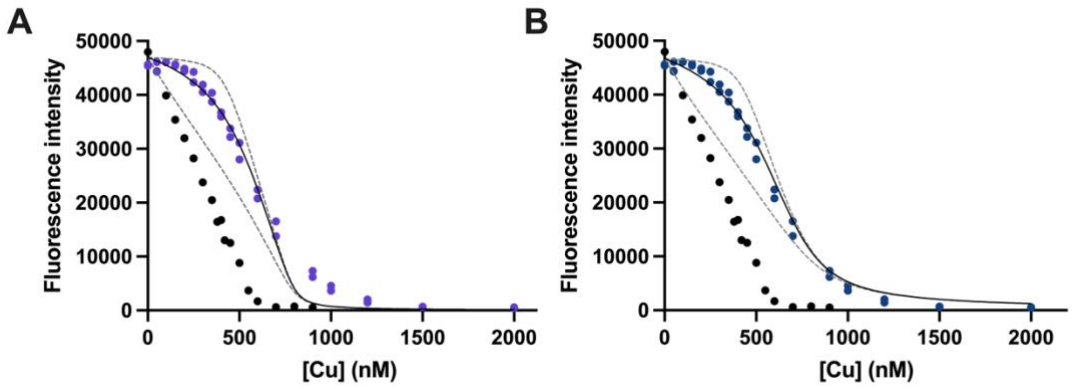

Figure 20 A Quenching of the fluorescence intensity of Zn-FZ3 in solution upon addition of Cu(II) in the absence (black) or presence (purple) of 400 nM Hst5 in 400 nM FZ3 and 500 nM Zn. The solid black line is the model fit to the data using Cu-FZ3 K_D = 9.1 × 10^{-11} M. Dashed lines are the 10-fold stronger and weaker fit of the model (Cu-Hst5 K_D = 1.3 × 10^{-8} M). **B** New fit of the data using Cu-FZ3 K_D = 9.1 × 10^{-10} M. Dashed lines are the 10-fold stronger and weaker fit of the model (Cu-Hst5 K_D = 1.55 × 10^{-9} M).

Finally, PAR (K_D = 1.85 × 10^{-13} M) was used to compete with Hst5 for Cu. PAR has peak absorbance at 420 nm due to *apo*-PAR, which decreased upon addition of Cu and increased absorbance at 512 nm corresponding to the formation of Cu-PAR. A clear endpoint was observed when 10 μM Cu was added

to 10 μM PAR, consistent with the expected stoichiometry of 1:1 Cu:PAR. The new absorbance at 512 nm was monitored to track the formation of Cu-PAR with (purple) and without (black) 200 μM Hst5 (Figure 21B). In the presence of Hst5, higher concentrations of Cu(II) were needed to saturate PAR, indicating the competition of Hst5 and PAR. The equilibrium model in equation 10 was fitted to the data on Dynafit giving the K_D = 6.63 × 10^{-13} M.

The dissociation constant of Cu-Hst5 sits in a similar range of the predicted Cu-AdcAI affinity. If Cu is imported via the AdcABC system, it may be possible that Hst5 limits non-specific Cu import into the cell in *S. pyogenes.* Furthermore, limitation of Cu import can be predicted in other species that require Cu as nutrient by knowing the affinity and concentration of the Cu import protein and the concentration of Hst5 *in vivo*.

$$Cu^{II}PAR + Hst5 \rightleftharpoons Cu^{II}Hst5 + PAR \qquad \text{(eq. 10)}$$

(512 nm) (420 nm) λ_{max}

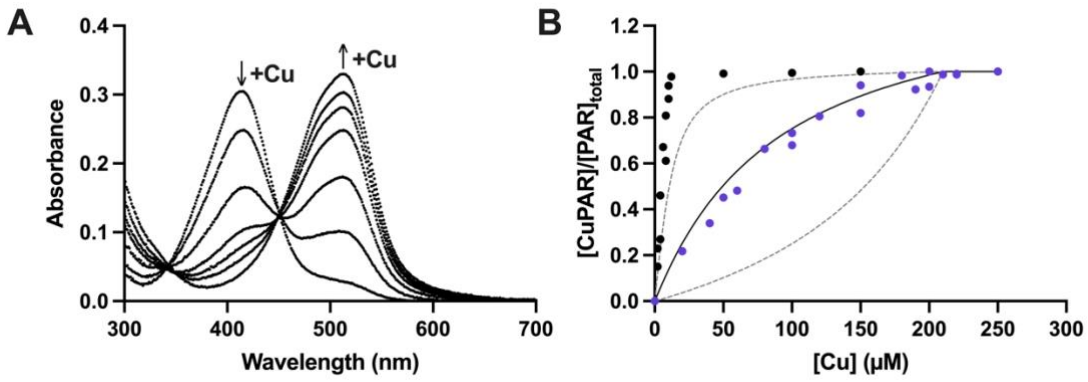

Figure 21 A Spectral change upon addition of Cu into PAR and Hst5. The maximum absorbance of *apo*-PAR at 420 nm decreases and Cu-PAR at 512 nm increases. **B** Normalised plot of the changes in solution absorbance of Cu-PAR at 512 nm upon addition of Cu in the absence (black) or presence (purple) of 200 μM Hst5 in 10 μM PAR. The solid black line is the model fit to the data and dashed lines are the 10-fold stronger and weaker fit of the model (Cu-Hst5 K_D = 6.63 × 10^{-13} M).

3.6 His3 is the important Cu(II) binding motif in Hst5

To confirm the amino acid that are involved in binding Cu(II), different variants of Hst5 where His residues are mutated to Ala were generated (Table 8). Affinities of these variants were measured under the same condition as the WT using PAR as a competitor (Figure 22). The competition between PAR and △H7, 8 and △H15, 18, 19 variants of Hst5 were indistinguishable from the competition curve with the WT Hst5. By contrast, the △H3 and △H3, 7 variants did not compete with PAR for binding Cu(II), indicating that they had lost their ability to bind Cu(II). Although the △H3, 7 variant had lost the ability to bind Cu, His7 is not likely to be involved in binding Cu(II), because the △H7, 8 did not lose Cu(II) binding. Therefore, His3 is the core ligand for binding Cu(II) in Hst5. The Zn binding affinities of these variants were not measured as the WT Hst5 already had a low affinity for Zn.

Table 8 Sequence of WT Hst5 and variants with mutations indicated in red.

Hst5 Variant	Sequence
WT	DSHAKRHHGYKRKFHEKHHSHRGY
△H3	ASAAKRHHGYKRKFHEKHHSHRGY
△H3, 7	DSAAKRAHGYKRKFHEKHHSHRGY
△H7, 8	DSHAKRAAGYKRKFHEKHHSHRGY
△H15, 18 ,19	DSHAKRHHGYKRKFAEKAASHRGY

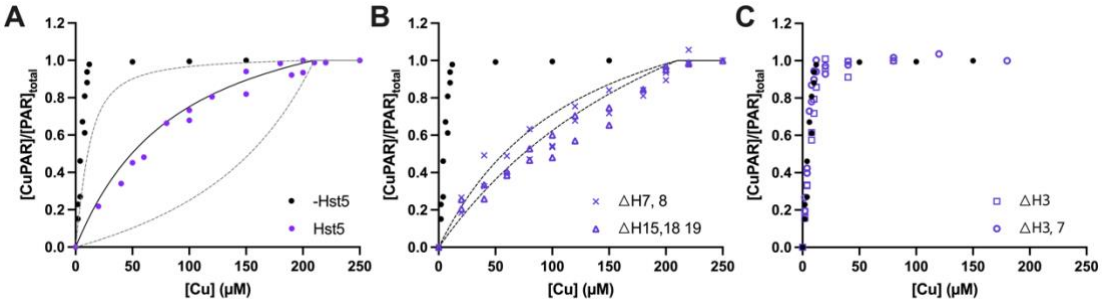

Figure 22 Normalised plot of the changes in solution absorbance of Cu-PAR at 512 nm upon addition of Cu in the absence (black) or presence (purple) of 200 μM Hst5 variants in 10 μM PAR. The solid black line is the model fit to the data. **A** Hst WT **B** △H7, 8 and △H15, 18, 19 are not affected in Cu binding and competes with PAR, **C** △H3 and △H3, 7 do not have the ability to bind Cu. All experiments were performed in 50 mM MOPS buffer pH 7.4.

3.7 Hst5 can rescue metal toxicity in GAS growth

To understand the role of Hst5 in changing metal availability, the effect of this peptide on the growth of *S. pyogenes* was examined. Colleagues in the Djoko lab have separately examined the hypothesis that Hst5 limits nutrient Zn availability using the *S. pyogenes* Δ*adcAI* mutant. Therefore, this work focused on the potential role of Hst5 in promoting metal toxicity instead. Hst5 was added to the culture media of *S. pyogenes* WT, △*copA,* and △*czcD* (Figure 23). The △*copA* mutant strain is impaired in Cu efflux, and the △*czcD* mutant strain is impaired in Zn efflux. Therefore, these mutants accumulate excessive intracellular metal leading to toxicity. These strains display a growth defect with added metal in the culture media.

First, the baseline effects of Cu and Zn on growth of each strain were examined in the absence of Hst5. In culture without Hst5, the WT was not affected by the increase of Cu or Zn, but the metal export mutants had attenuated growth by the increase of concentration of the cognate metals. The growth of the Δ*copA* mutant is attenuated by any added Cu but Δ*czcD* mutant is only affected by at least 10 μM Zn in the culture (Figure 23). It is likely that because Zn is required in the cell in *S. pyogenes*, the addition of Zn in the △*czcD* mutant is not as hugely affected as the addition of Cu in the △*copA* mutant.

In the same conditions, 50 μM of Hst5 in the culture rescues growth of the Δ*copA* mutant and Δ*czcD* mutant from Cu or Zn toxicity (Figure 23). These results indicate that, contrary to the original hypothesis, Hst5 did not promote metal toxicity. It is likely that the added Hst5 in the media is binding and buffering the excess Cu or Zn and decreases the metal being imported into the cell, preventing metal toxicity. The buffering of Cu is not surprising as the Cu affinity of Hst5 is high, and growth of the Δ*copA* mutant is fully recovered even up to 20 μM added Cu in the media. In the Δ*czcD* mutant, Hst5 is also showing mild protective effects from Zn toxicity even though it binds with less than a micromolar affinity. Any added Zn does not seem to affect the growth until 10 μM Zn. There is a slight delay in growth which is recovered and reaches an optical density that is indistinguishable from the WT growth. Therefore, the presence of 50 μM Hst5 is capable of binding sufficient concentration of Zn in the media to reduce the toxicity due to excessive Zn.

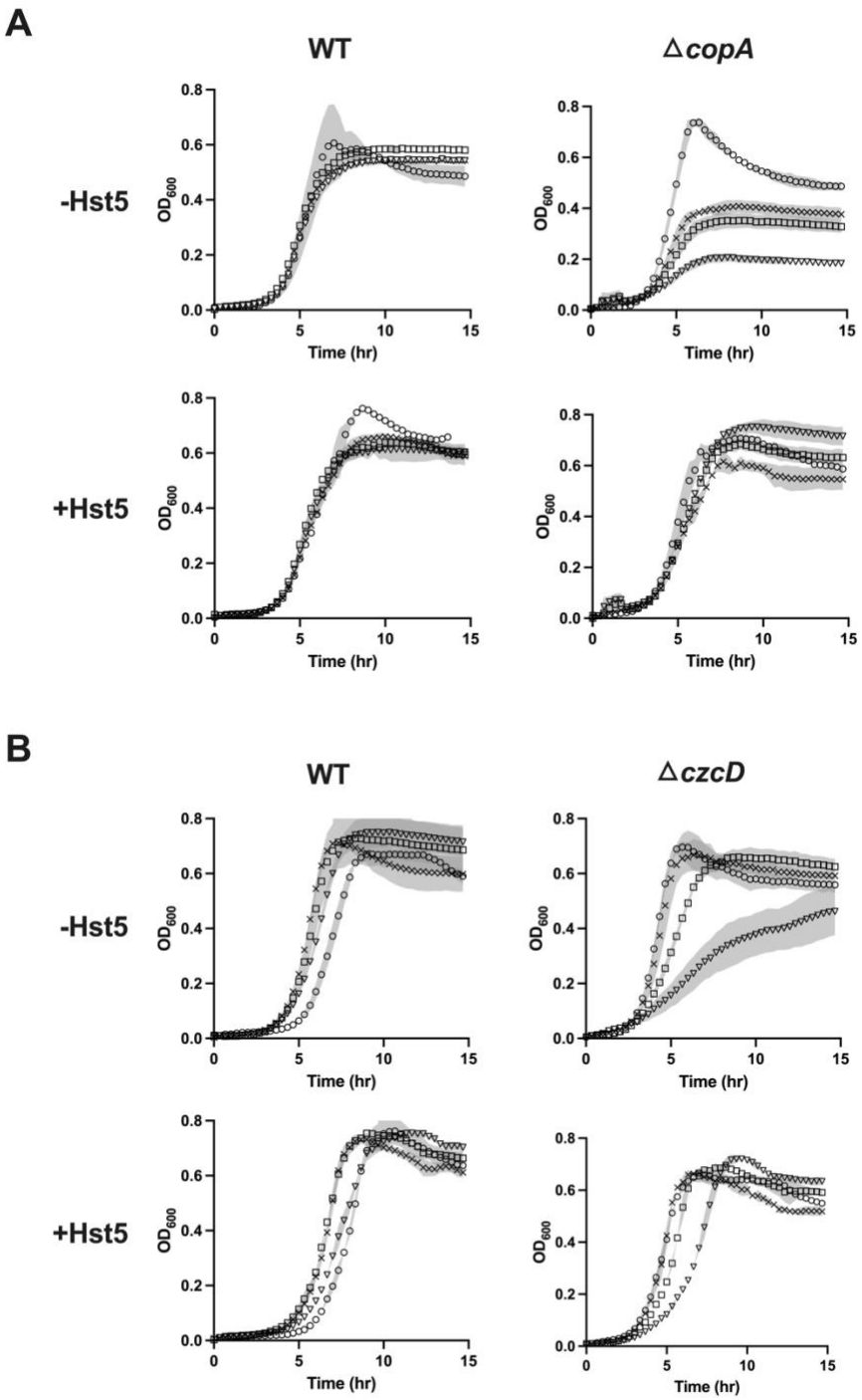

Figure 23 A Effects of Cu (0, 5, 10, 20 μM, O, X, □, ▽) and Hst5 on growth of *S. pyogenes* WT and △*copA*. **B** Effects of Zn (0, 2, 5, 10 μM, O, X, □, ▽) and Hst5 on growth of *S. pyogenes* WT and △*czcD.* Adding WT Hst5 (50 μM) in the culture can rescue growth of both mutants. The symbols are the mean of two replicates and shaded area showing the standard deviation.

To examine the important residues for the protective effect of Hst5 during Cu toxicity, the four Hst5 variants were added to the same culture condition in △*copA* (Figure 24). As we saw the loss of the ability to bind Cu in the variants that contained mutation at His3, it was expected that those variants would not restore growth in Cu toxicity. △H3 and △H3, 7 variants did not rescue growth of the △*copA* mutant in excess Cu, while the other two variants △H7, 8 and △H15, 18, 19 restored growth as the Hst5 WT (Figure 24). These results reconfirm the importance of the His3 in Hst5 in Cu binding.

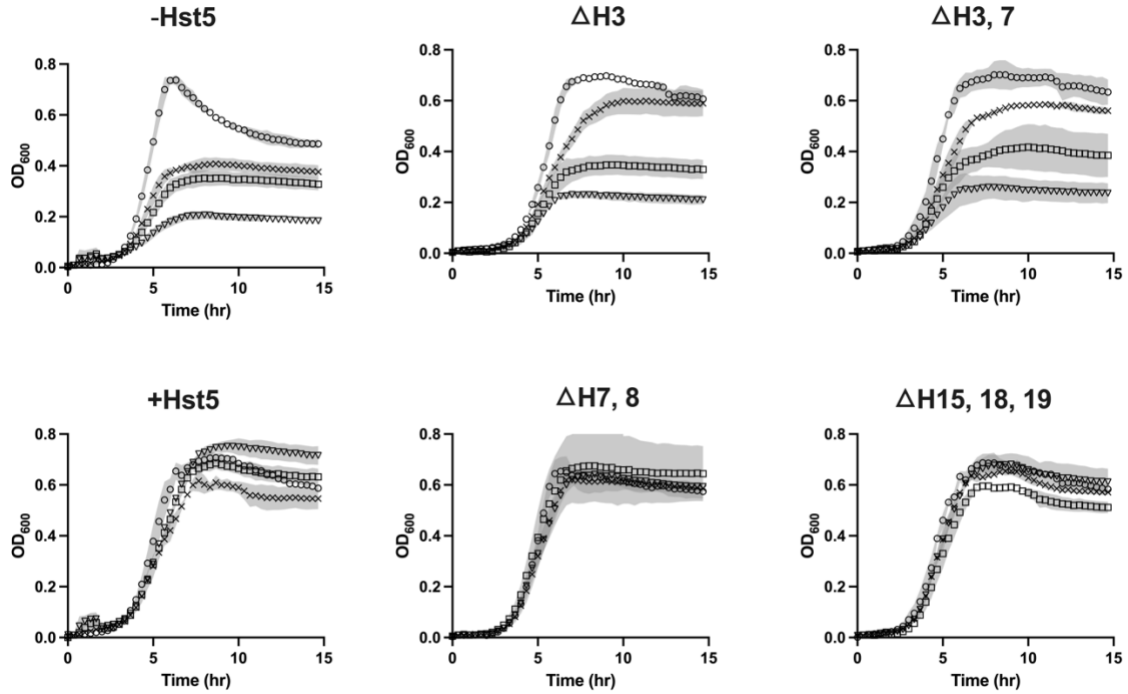

Figure 24 Effects of Hst5 variants on growth of the *S. pyogenes* △*copA* mutant under Cu toxicity. Growth is not restored in Hst5 variants with H3A mutation. The symbols are the mean of two replicates and shaded area showing the standard deviation. (Cu: 0, 5, 10, 20 μM, O, X, □, ▽)

4. Discussion

This study investigated the characteristics of the Zn and Cu binding of Hst5 in parallel to the Zn import system of the model organism *S. pyogenes*. Hst5 is known to be an antimicrobial peptide, especially well-understood as an antifungal peptide, most heavily studied against *C. albicans*. The conserved metal binding motifs suggest a metal dependent role of Hst5, but the mechanism of the metal dependence is yet to be determined. However, Stewart et al. have shown that Hst5 does not kill *Streptococci* [98], in contrast to the killing effects seen in fungal and ESKAPE pathogens, leaving the antimicrobial activity of Hst5 in question. This project hypothesised that Hst5 is potentially involved in nutritional immunity.

4.1 Measurements of metal binding using equilibrium competition against a colourimetric probe.

When using colourimetric probes (L) as a competitor to evaluate metal (M) binding to a protein (P), it is important to assess the entire solution spectra rather than the single wavelength of the peak absorbance. This approach helps ensure that the metal binds directly to the probe (ML or ML_2) without side reactions such as formation of a ternary complex with the competing protein. Direct binding of metal to the probe should only produce two peaks in the spectra: one for the *apo*-probe (L) and one for the *holo*-probe (ML or ML_2). The absorbance intensity of each peak will change in proportion to the concentration of metal added. However, the wavelength of each peak should not change because the chemical nature of the species responsible for each peak (L, ML, or ML_2) remains unchanged. In addition, the peaks should crossover at the same points at any concentration of metal added. These crossover points are known as the isosbestic points.

For example, as shown in the titration of Cu into PAR in Figure 25A, two peaks are present in all the spectra at 420 and 512 nm, corresponding to the *apo*- (L) and *holo*-forms of this probe (ML). In addition, two isosbestic points can be clearly observed at 338 and 450 nm (Figure 25A, red circles). The presence of these isosbestic points confirms that the addition of Cu into a solution of *apo*-PAR (L; peak at 420 nm) generates Cu-PAR (ML; peak at 512 nm) as the sole reaction product. By contrast, repeating this titration in the presence of AdcAI (P; Figure 25B, red) induced a clear change in the shape of the *holo*-PAR spectrum and a shift in the *holo*-PAR peak wavelength from 512 nm to 520 nm (Figure 25B). In

addition, the isosbestic point at 338 nm is lost. Both features suggest the formation of potential ternary complexes between AdcAI, PAR, and Cu. As the exact ternary species cannot be identified from the competition assay, for example whether it was a 1:1:1 PAR:Cu:AdcAI complex or another species, the data cannot be reliably fitted to an equilibrium competition model shown in equation 11.

$$2\ Cu^{II}PAR + AdcAI \rightleftharpoons 2\ Cu^{II}AdcAI + 2PAR \qquad \text{(eq. 11)}$$

(512 nm) (420 nm) λ_{max}

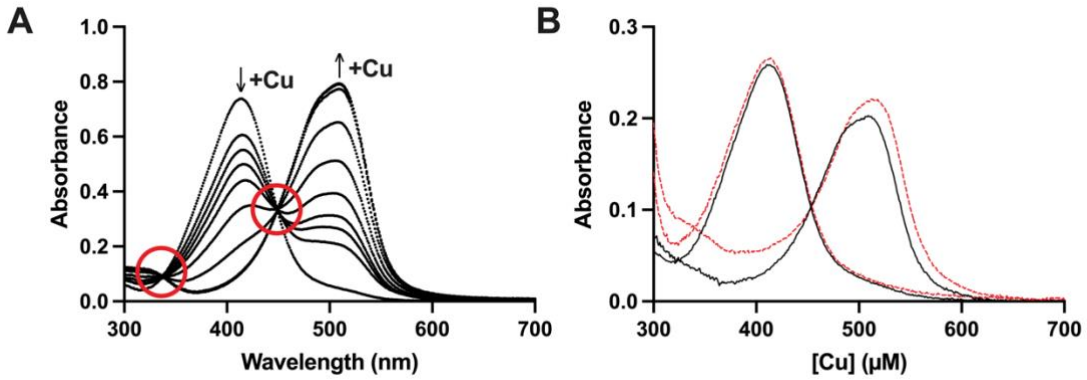

Figure 25 A Change of solution absorbance upon addition of Cu into PAR. Red circles indicating the isosbestic points. **B** Addition of AdcAI (red) to PAR and Cu (black) causes a spectral shift and no longer forms isosbestic points.

4.2 Zn binding to AdcAI

This thesis reports the metal-binding affinities for the *Streptococcal* Zn uptake lipoprotein AdcAI, measured using equilibrium competition assays against colourimetric and flurometric probes with varying affinities. The results confirm a previous model [66] that AdcAI binds two Zn atoms with distinct affinities. However, the affinity values obtained in this work (K_D = 5.3 × 10^{-13} M and 6.7 × 10^{-8} M) (Figure 16 and 17) are approximately 200000 and 40 times higher when compared with those reported previously by Cao et al., (93 × 10^{-9} M and 1.1 - 2.6 × 10^{-6} M). These literature values were obtained using ITC, which can lack sensitivity, especially for measuring tight binding. The concentrations of

protein and metal required to generate sufficient heat change for detection are typically much higher than the K_D values of the metalloprotein. In addition, heat change can report events outside metal binding to a protein [99]. For example, side reactions involving metal binding to the buffer can often produce a heat change. Therefore, ITC often only provides upper limits of the K_D and therefore lower limits of the affinity. Conducting equilibrium competition assays with competitors of known affinities provide more accurate K_D values, as long as an effective competition between the protein and the probe for the metal is observed. For example, the affinity of the AdcAI tight site for Zn could not be accurately estimated using MF2 as a competitor, since AdcAI outcompeted the probe (Figure 16B). The affinity of this site was better estimated using Quin2 as the competitor, since an effective competition was observed between AdcAI and Quin2 (Figure 17B).

4.3 Zn binding properties of Hst5

Previous studies have shown that Hst5 can bind up to three Zn ions. ITC measurements yielded K_D = 1×10^{-5} M for the tightest bound Zn and 1×10^{-4} M for the two more weakly bound Zn. A previous study also showed an effective competition between Hst5 and Zincon, a Zn-binding probe with much lower affinity ($K_D = 1.26 \times 10^{-5}$ M) [54]. However, it is important to note here that this competition with Zincon was performed in phosphate buffer. When used at millimolar concentrations, phosphate can become competitive for binding Zn ($K_D = 4.0 \times 10^{-3}$ M) [100]. Therefore, the observed competition between Hst5 and Zincon should have accounted for phosphate as a third competitor in the system. Nevertheless, based on the ability of Hst5 to bind Zn, it was hypothesised that this peptide plays a role in nutritional immunity, either by limiting nutrient Zn availability to *S. pyogenes* and promoting bacterial Zn starvation, or by enhancing the supply of excess Zn to *S. pyogenes* and promoting bacterial Zn toxicity.

Work by colleagues in the Djoko lab indicated that, contrary to the original hypothesis, addition of Hst5 into *S. pyogenes* cultures did not induce a Zn starvation phenotype [98]. Hst5 did not suppress growth of the *S. pyogenes adcAI* mutant strain lacking the high-affinity Zn uptake lipoprotein AdcAI. Hst5 also did not upregulate expression of AdcR-regulated genes such as *adcAI* gene.

Likewise, work presented in this thesis indicated that Hst5 did not promote Zn toxicity in *S. pyogenes*. Addition of Hst5 did not enhance the Zn-dependent growth inhibition of the Δ*czcD* mutant lacking the

primary Zn efflux facilitator (Figure 23). Work by colleagues in the Djoko lab further confirmed that Hst5 did not increase the Zn-dependent upregulation of the *czcD* gene [98]. Instead, Hst5 appeared to protect the Δ*czcD* mutant effects from excessive Zn (Figure 23), albeit only weakly.

Results from the Djoko lab suggest that Hst5 does not promote Zn starvation in *S. pyogenes* [98]. This thesis provides a molecular mechanism for these observations. As described in the literature, the affinity of Hst5 to Zn was weak at K_D = 8.3 × 10^{-6} M. Consistent with this weak affinity, micromolar concentrations of Zn-Hst5 complex did not survive elution from a desalting column (Figure 18A). This affinity value for Zn-Hst5 is 16000000 times weaker than the tight site of AdcAI and 124 times weaker than the weak site of AdcAI. Consistent with this hypothesis, while AdcAI clearly competed with the fluorometric probe MF2, Hst5 did not (Figure 18B). These relative affinities suggest that Hst5 does not compete with AdcAI for binding Zn, which would explain why Hst5 does not starve *S. pyogenes* of nutrient Zn.

The weak affinity of Zn to Hst5 also explains why Hst5 does not promote Zn toxicity. The culture medium employed in streptococcal growth assays contains high concentrations of phosphate and other amino acids such as His and Glu, all of which can compete for binding Zn. Therefore, it is likely that the Zn-Hst5 complex is not stable in the culture medium. Instead, the Zn-Hst5 complex likely dissociates in the culture medium as a result of competition with other potential Zn-binding molecules. Therefore, the model in which a Zn-Hst5 complex enters the cytoplasm (Figure 26) and drives accumulation of intracellular Zn is unlikely.

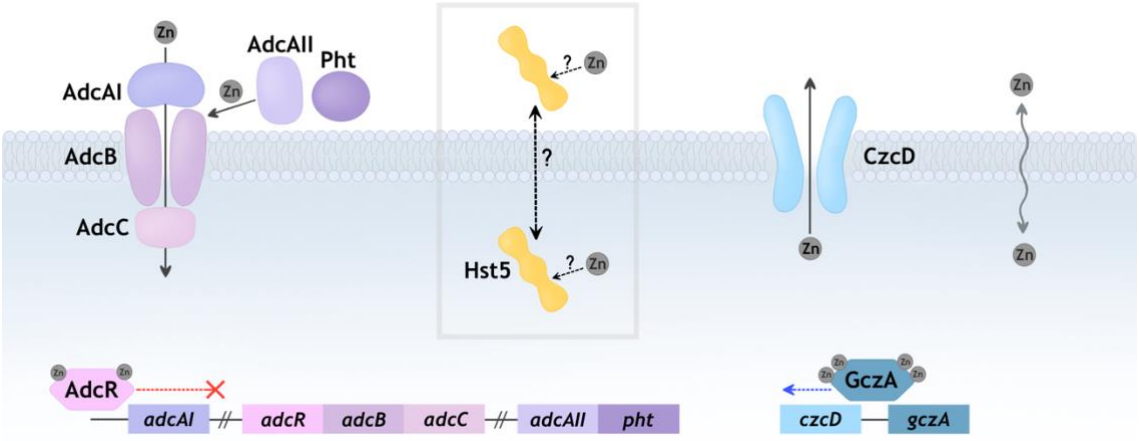

Figure 26 Zn homeostasis system in *S. pyogenes* and hypothesised role(s) of Hst5.

As growth media components become depleted, for example during the later phase of bacterial growth, the lack of competitors may then allow binding of Zn to the Hst5 peptide. This likely explains why a slight protective effect is observed in Figure 23, where growth of the Δ*czcD* mutant of *S. pyogenes* in the presence of Zn is improved slightly.

4.4 Cu binding properties of Hst5

It has been previously studied that Hst5 binds Cu(II) at the ATCUN site with affinity of K_D = 7.94 × 10^{-12} M by competition assay with NTA and two Cu(I) at each *bis*-His motif with an affinity of K_D = 2.51 × 10^{-8} M, determined by competition with ferrozine [52]. The Cu(II) affinity of Hst5 was measured with three different probes, NTA to repeat the experiments from the previous study of Conklin et al., FZ3, and PAR. Competition assay with PAR provides the best estimate of the affinity, compared with NTA and FZ3. The competition data with FZ3 (Figure 20A) could not be fitted with the equilibrium model with the currently known affinity of Cu-FZ3. As seen in Figure 19, the maximum peak absorbance of Cu-NTA does not plateau even when the ligands are saturated with Cu(II), likely a result of Cu(II)-buffer interactions.

As Hst5 binds Cu with a high affinity, of K_D = 6.63 × 10^{-13} M (Figure 21), it was hypothesised that this peptide has a role in nutritional immunity by limiting Cu availability and promoting Cu starvation, or by enhancing the supply of excess Cu and promote Cu toxicity. However, *S. pyogenes* is not thought to use Cu as a nutrient and therefore Cu starvation cannot disrupt viability, leaving only the model of Hst5 promoting Cu toxicity as the potential role of Hst5 in nutritional immunity for Cu.

Work by colleagues in the Djoko lab indicated that addition of Hst5 into *S. pyogenes* culture did not induce a Cu toxicity phenotype [98]. Hst5 did not upregulate expression of *copA*, the CopY-regulated gene. In contrast to the hypothesis, the addition of Hst5 rather reduced the expression of *copA* which is indicative of reduced Cu stress.

Similarly, the work presented in this thesis show that Hst5 did not promote Cu toxicity in *S. pyogenes*. The addition of Hst5 did not enhance the Cu-dependent growth inhibition of the Δ*copA* mutant lacking the Cu efflux pump (Figure 23). This study also showed the protective effects of Hst5 in the growth of Δ*copA* mutant in the presence of excessive Cu (Figure 23).

By examining the different Hst5 variants, it was determined that Cu(II) binding was relevant and not Cu(I) binding. Therefore, the Cu(II) site of Hst5 is crucial in the role of buffering excessive Cu in the growth of *S. pyogenes*. Since Cu(II) is not thought to exist in the reducing cytoplasm, it is likely that Hst5 binds extracellular Cu and suppresses the entry of Cu in the cytoplasm of *S. pyogenes*. This proposal is supported by the work from the Djoko lab, with ICP MS analysis showing lower intracellular Cu levels in Hst5 treated cells. Therefore, the model in which a Cu-Hst5 complex enters the cytoplasm (Figure 27) and drives accumulation of intracellular Cu is unlikely.

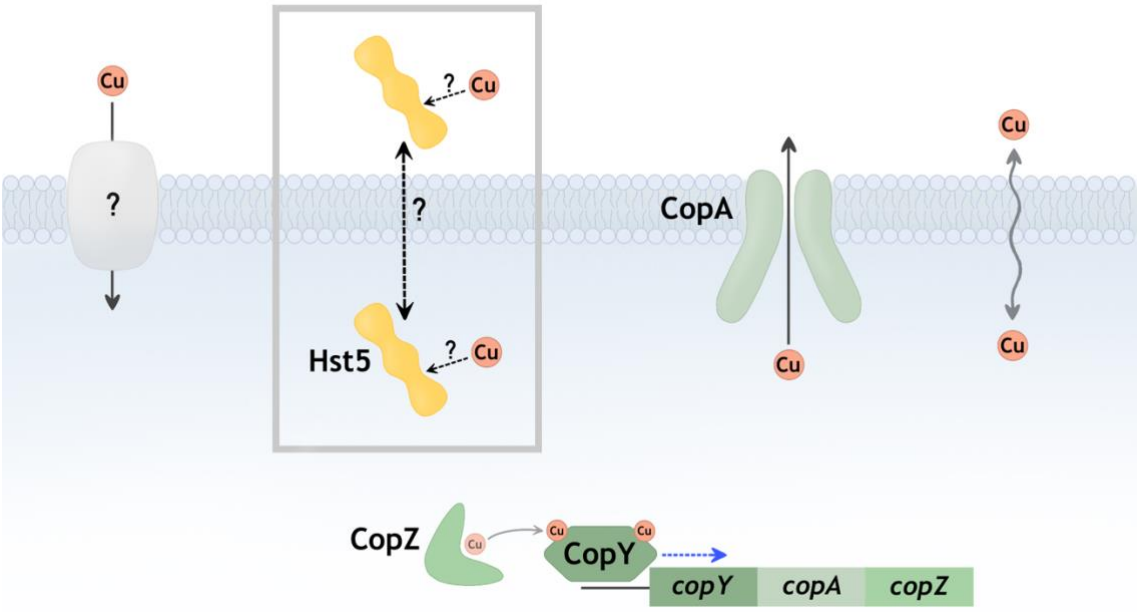

Figure 27 Cu homeostasis system in *S. pyogenes* and hypothesised role(s) of Hst5.

4.5 The likely physiological role of Hst5

Hst5 has been proposed to bind metals like Zn(II), Ni(II), Cu(I) and Cu(II) [52, 54, 101]. Metal binding AMPs can have two major modes of action that is dependent on metal binding. The first is by the metal functioning as a cofactor that switches “on” the activity of the AMP, or the second by participating in nutritional immunity. Nutritional immunity was thought to be limited to inducing starvation of nutrients from the invading pathogen, but it has been observed that animal hosts can manipulate the metal availability at the site of infection to cause metal poisoning. Hence, the metal binding AMP can also have a role in delivering excessive metal ions to the invading pathogen and induce metal toxicity.

Another mode of action that involves metals in the action of AMPs can be synergistic effects of the metal ion and the AMP, that does not involve binding of the metal. This can be observed when there is an enhanced antimicrobial effect of the AMP in the presence of the metal as they both together promote cell death or damage but does not require binding and formation of a complex does not occur in the cell.

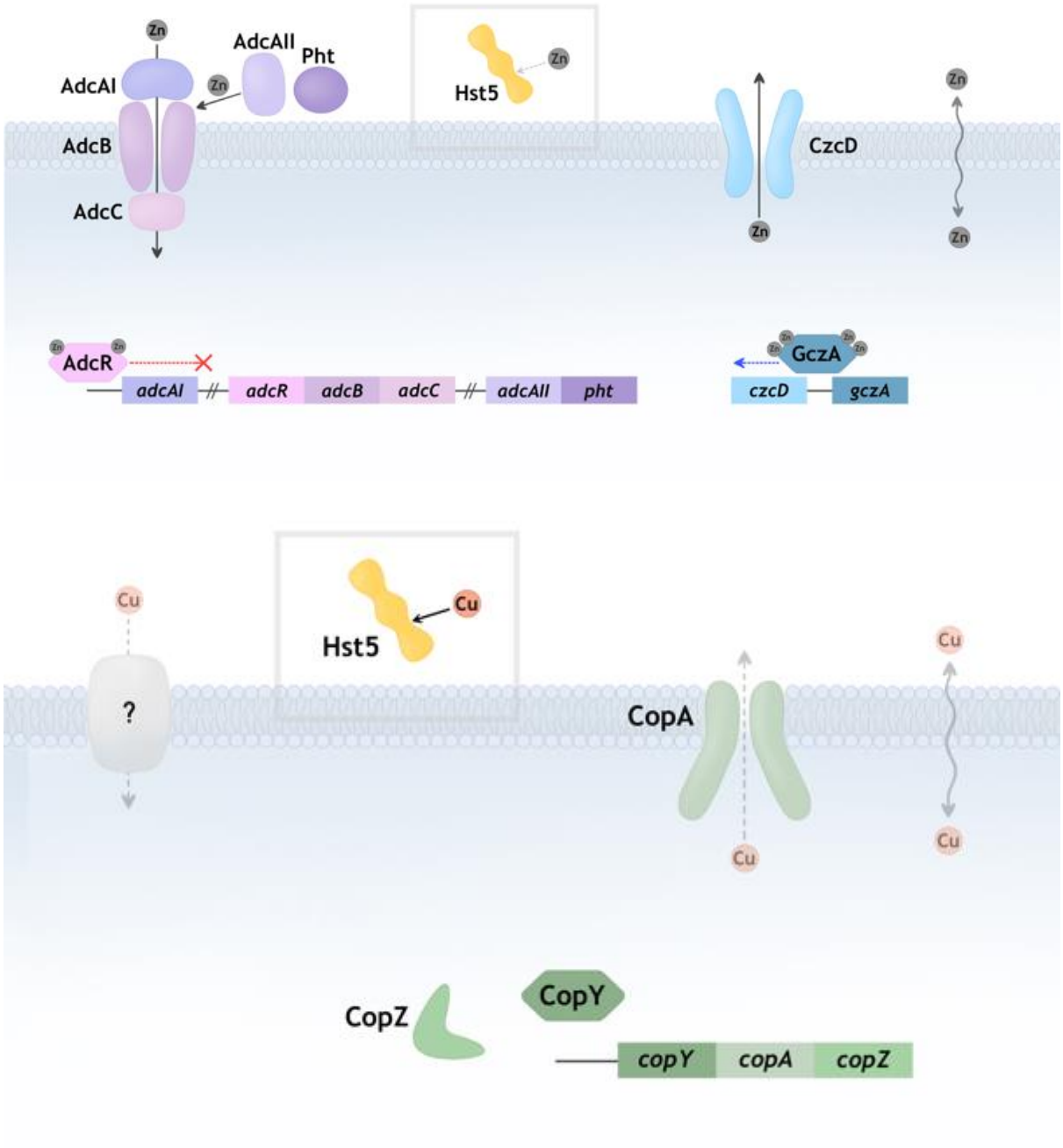

Figure 28 The proposed model of Hst5 in *S. pyogenes.*

It is clear from the results from this study and from parallel work done in the Djoko lab [98] that Hst5 does not act as a metal-dependent antibacterial agent, whether through direct metal binding to the AMP or *via* synergistic effects, against the pathogen *S. pyogenes*. Instead, Hst5 appears to play a role in influencing metal availability, especially Cu, to *S. pyogenes*, and potentially other oral streptococci (Figure 28).

Hst5 has been proposed as an antifungal AMP that requires Cu as a cofactor [52]. The proposed antifungal mechanism involves the internalisation of the peptide *via* energy-dependent pathways by interacting with the fungal membrane proteins, which makes the fungal pathogen a specific target. However, in this study, it was shown that Hst5 remains extracellular of the bacteria and binds excessive Zn and Cu in the environment. The proportion of *Streptococci* in the oral microbiome can be up to 60%, depending on the site and individual. As reduced Cu availability does not negatively influence the growth of streptococci, the chelation or buffering effect of Hst5 is likely beneficial in maintaining a healthy population of the streptococci in the oral cavity. The constant secretion of Hst5 by the salivary glands into the saliva may help adjust Cu availability in the oral cavity so that it is kept below the threshold at which it can cause Cu poisoning in resident streptococci. Oral Cu availability may fluctuate due to consumption of food or food supplement, and Hst5 may buffer this metal as seen in this study.

Whether Hst5 has a role in limiting Cu availability to other oral microbes that may require Cu as a nutrient still remains as a question. If the affinity of Hst5 to Cu and the concentration of Hst5 present in the saliva are high enough to outcompete the Cu import systems in these microbes, then these microbes will starve. It is possible that this is a mechanism by which the growth of potential oral pathogens is suppressed, but how this is balanced with growth of potential beneficial oral microbes is not known.

5. Future work

5.1 Generation of *apo*-AdcAII and characterisation

For future studies, understanding AdcAII could provide deeper knowledge of the Zn homeostasis system of *S. pyogenes*. This study did not continue with identifying the Zn binding characteristics of AdcAII due to time constraints as generation of *apo*-AdcAII required an additional step of overnight dialysis with excessive EDTA [102] and the individually measured affinities of AdcAI and Hst5 have answered the hypothesis of whether Hst5 can promote Zn starvation. However, the role of AdcAII in Zn acquisition remains unclear, why *S. pyogenes* requires both AdcAI and AdcAII and how AdcAII interacts with Pht and AdcB to import extracellular Zn. Therefore, understanding AdcAII may provide insight to how *S. pyogenes* acquires Zn and how it may be inhibited with antimicrobial peptides.

5.2 Direct competition of AdcAI and Hst5 for Zn and Cu

Although this study has shown that Hst5 would not be able to outcompete AdcAI and induce metal starvation in *S. pyogenes*, a direct competition of AdcAI and Hst5 for Zn would be another method to confirm that Hst5 would not be able to bind Zn in physiological conditions where high affinity metal import proteins are present. This can be achieved by incubating isolated AdcAI, Hst5 and Zn at physiologically relevant concentrations, separate AdcAI and Hst5 by size exclusion chromatography and assess where the Zn is bound as it was done in this study, by denaturing the protein with 6 M guanidine chloride and using PAR. The size of AdcAI is approximately 20-fold larger than Hst5, so size exclusion chromatography will be the easiest method to separate the two proteins.

5.3 Hst5 inducing Cu starvation in other oral microbes

The metal dependent role of Hst5 on Cu and Zn was all examined and has been eliminated except one possibility, Hst5 as a Cu chelator and cause Cu starvation. *S. pyogenes* was the model organism in this study as GAS is the most common oral microbe, but it does not require Cu for growth or virulence. Hst5 may have a role in limiting Cu availability in the smaller proportion of the oral microbiome or Cu-requiring pathogenic bacteria and limit the overgrowth of those species.

5.4 Hst5 binding other metals

In this study, only the Zn and Cu(II) binding of Hst5 was characterised. However, it has been seen that Hst5 can bind Ni and previous studies had shown that it can bind up to 10 Fe atoms. Other *d-block* divalent metals such as Co and Mn could also potentially bind Hst5, as many His containing proteins and peptides do, and have an antimicrobial role. The affinity and *in vitro* activity of Hst5 dependent on these different metals can be examined by competition assays, in the same method as it was done in this study.

6. References

[1] D. Markov, T. Naryshkina, A. Mustaev and K. Severinov, "A zinc-binding site in the largest subunit of DNA-dependent RNA polymerase is involved in enzyme assembly," *Genes and Development,* vol. 13, no. 18, pp. 2439-2448, 1999.

[2] M. P. Hensley, D. L. Tierney and M. W. Crowder, "Zn(II) Binding to Escherichia coli 70S Ribosomes," *Biochemistry,* vol. 50, no. 46, pp. 9937-9939, 2011.

[3] V. M. Krishnamurthy, G. K. Kaufman, A. R. Urbach, I. Gitlin, K. L. Gudiksen, D. B. Weibel and G. M. Whitesides, "Carbonic Anhydrase as a Model for Biophysical and Physical-Organic Studies of Proteins and Protein–Ligand Binding," *Chemical Review,* vol. 108, no. 3, pp. 946-1051, 2008.

[4] T. Tsukihara, H. Aoyama, E. Yamashita, T. Tomizake, H. Yamaguchi, K. Shinzawa-Itoh, R. Nakashima, R. Yaono and S. Yoshikawa, "The Whole Structure of the 13-Subunit Oxidized Cytochrome c Oxidase at 2.8 Å," *Science,* vol. 272, no. 5265, pp. 1136-1144, 1996.

[5] P. I. Oteiza, "Zinc and the modulation of redox homeostasis," *Free Radical Biology and Medicine,* vol. 53, no. 9, pp. 1748-1759, 2012.

[6] H. Beinert, R. H. Holm and E. Münck, "Iron-Sulfur Clusters: Nature's Modular, Multipurpose Structures," *Science,* vol. 277, no. 5326, pp. 653-659, 1997.

[7] T. Palzkill, "Metallo-β-lactamase structure and function," *Annals of the New York Academy of Sciences,* vol. 1277, pp. 91-104, 2013.

[8] C. O. Pabo, E. Peisach and R. A. Grant, "Design and Selection of Novel Cys2His2 Zinc Finger Proteins," *Annual Review of Biochemistry,* vol. 70, pp. 313-340, 2001.

[9] H. Tamano, Y. Koike, H. Nakada, Y. Shakush and A. Takeda, "Significance of synaptic Zn2+ signaling in zincergic and non-zincergic synapses in the hippocampus in cognition," *Journal of Trace Elements in Medicine and Biology,* vol. 38, pp. 93-98, 2016.

[10] N. D'Ambrosi and L. Rossi, "Copper at synapse: Release, binding and modulation of neurotransmission," *Neurochemistry International,* vol. 90, pp. 36-45, 2015.

[11] H. Irving and R. J. P. Williams, "The Stability of Transition-metal Complexes," *Journal of The Chemical Society,* pp. 3192-3210, 1953.

[12] D. Osman, M. A. Martini, A. W. Foster, J. Chen, A. J. P. Scott, R. J. Morton, J. W. Steed, E. Lurie-Luke, T. G. Huggins, A. D. Lawrence, E. Deery, M. J. Warren and P. T. Chivers, "Bacterial sensors define intracellular free energies for correct enzyme metalation," *Nature Chemical Biology,* vol. 15, pp. 241-249, 2019.

[13] P. Chandrangsu, C. Rensing and J. D. Helmann, "Metal homeostasis and resistance in bacteria," *Nature Reviews Microbiology,* vol. 15, pp. 338-350, 2017.

[14] M. W. Terhune and H. H. Sandstead, "Decreased RNA Polymerase Activity in Mammalian Zinc Deficiency," *Science,* vol. 177, no. 4043, pp. 68-69, 1972.

[15] Y. Li, M. R. Sharma, R. K. Koripella, Y. Yang, P. S. Kaushal, Q. Lin, J. T. Wade, T. A. Gray, K. M. Derbyshire, R. K. Agrawal and A. K. Ojha, "Zinc depletion induces ribosome hibernation in mycobacteria," *PNAS,* vol. 115, no. 32, pp. 8191-8196, 2018.

[16] J. Y. Duffy, G. J. Overmann, C. L. Keen, M. S. Clegg and G. P. Daston, "Cardiac Abnormalities Induced by Zinc Deficiency AreAssociated With Alterations in the Expression of GenesRegulated by the Zinc-Finger Transcription FactorGATA-4," *Developmental and Reproductive Toxicology,* vol. 71, no. 2, pp. 102-109, 2004.

[17] L.-J. Cartier, Y. Ohira, M. Chen, R. W. Cuddihee and J. O. Holloszy, "Perturbation of Mitochondrial Composition in Muscle by Iron Deficiency," *The Journal of Biological Chemistry,* vol. 261, no. 29, pp. 13827-13832, 1986.

[18] T. A. Rouault and W. H. Tong, "Iron-sulfur cluster biogenesis and human disease," *Trends in Genetics,* vol. 24, no. 8, pp. 398-407, 2008.

[19] J. A. Tainer, E. D. Getzoff, J. S. Richardson and D. C. Richardson, "Structure and mechanism of copper, zinc superoxide dismutase," *Nature,* vol. 306, pp. 284-287, 1983.

[20] C. Walling and A. Goosen, "Mechanism of the ferric ion catalyzed decomposition of hydrogen peroxide. Effect of organic substrates," *Journal of the American Chemical Society,* vol. 95, no. 5, pp. 2987-2991, 1973.

[21] M. Mestivier, J. R. Li, A. Camy, C. Frangville, C. Mingotaud, F. Benoît-Marquié and J.-D. Marty, "Copper-Based Hybrid Polyion Complexes for Fenton-Like Reactions," *Chemistry A European Journal,* vol. 26, no. 62, pp. 14152-14158, 2020.

[22] A. Giachino and K. J. Waldron, "Copper tolerance in bacteria requires the activation of multiple accessory pathways," *Molecular Microbiology,* vol. 114, no. 3, pp. 377-390, 2020.

[23] L. Macomber and J. A. Imlay, "The iron-sulfur clusters of dehydratases are primary intracellular targets of copper toxicity," *PNAS,* vol. 106, no. 20, pp. 8344-8349, 2009.

[24] S. Tottey, C. J. Patterson, L. Banci, I. Bertini, I. C. Felli, A. Pavelkova, S. J. Dainty, R. Pernil, K. J. Waldron, A. W. Foster and N. J. Robinson, "Cyanobacterial metallochaperone inhibits deleterious side reactions of copper," *PNAS,* vol. 109, no. 1, pp. 95-100, 2012.

[25] M. D. L. Johnson, T. E. Kehl-Fie and J. W. Rosch, "Copper intoxication inhibits aerobic nucleotide synthesis in Streptococcus pneumoniae," *Metallomics,* vol. 7, no. 5, pp. 786-794, 2015.

[26] K. Mounaji, M. Vlassi, N.-E. Erraiss, M. Wegnez, A. Serrano and A. Soukri, "In vitro effect of metal ions on the activity of two amphibian glyceraldehyde-3-phosphate dehydrogenases: potential metal binding sites," *Comparative Biochemistry and Physiology Part B: Biochemistry and Molecular Biology,* vol. 135, no. 2, pp. 241-254, 2003.

[27] M. I. Hood and E. P. Skaar, "Nutritional immunity: transition metals at the pathogen–host interface," *Nature Revies Microbiology,* vol. 10, pp. 525-537, 2012.

[28] M. B. Brophy and E. M. Nolan, "Manganese and Microbial Pathogenesis: Sequestration by the Mammalian Immune System and Utilization by Microorganisms," *ACS Chemical Biology,* vol. 10, no. 3, pp. 641-651, 2015.

[29] C. Champaiboon, K. J. Sappington, B. D. Guenther, K. F. Ross and M. C. Herzberg, "Calprotectin S100A9 Calcium-binding Loops I and II Are Essential for Keratinocyte Resistance to Bacterial Invasion," *The Journal of Biological Chemistry,* vol. 284, no. 11, pp. 7078-7090, 2009.

[30] D. M. Gagnon, M. B. Brophy, S. E. J. Bowman, T. A. Stich, C. L. Drennan, R. D. Britt and E. M. Nolan, "Manganese Binding Properties of Human Calprotectin Under Conditions of High and Low Calcium: X-ray Crystallographic and Advanced EPR Spectroscopic Analysis," *Journal of the American Chemical Society,* vol. 137, no. 8, pp. 3004-3016, 2015.

[31] T. G. Nakashige, B. Zhang, C. Krebs and E. M. Nolan, "Human calprotectin is an iron-sequestering host-defense protein," *Nature Chemical Biology,* vol. 11, pp. 765-771, 2015.

[32] A. N. Besold, B. A. Gilston, J. N. Radin, C. Ramsoomair, E. M. Culbertson, C. X. Li, B. P. Cormack, W. J. Chazin, T. E. Kehl-Fie and V. C. Culotta, "Role of Calprotectin in Withholding Zinc and Copper from Candida albicans," *Infection and Immunity,* vol. 86, no. 2, 2018.

[33] B. D. Corbin, E. H. Seeley, A. Raab, J. FeldMann, M. R. Miller, V. J. Torres, K. L. Anderson, B. M. Dattilo, P. M. Dunman, R. Gerads, R. M. Caprioli, W. Nacken, W. J. Chazin and E. P. Skaar, "Metal Chelation and Inhibition of Bacterial Growth in Tissue Abscesses," *Science,* vol. 319, no. 5865, pp. 962-965, 2008.

[34] R. Golonka, B. S. Yeoh and M. Vijay-Kumar, "The Iron Tug-of-War between Bacterial Siderophores and Innate Immunity," *Journal of Innate Immunity,* vol. 11, no. 3, pp. 249-262, 2019.

[35] C. White, J. Lee, T. Kambe, K. Fritsche and M. J. Petris, "A Role for the ATP7A Copper-transporting ATPase in Macrophage Bactericidal Activity," *Journal of Biological Chemistry,* vol. 284, no. 49, pp. 33949-33956, 2009.

[36] G. Porcheron, A. Garénaux, J. Proulx, M. Sabri and C. M. Dozois, "Iron, copper, zinc, and manganese transport and regulation in pathogenic Enterobacteria: correlations between strains, site of infection and the relative importance of the different metal transport systems for virulence," *Frontiers in Cellular and Infection Microbiology,* vol. 3, p. 90, 2013.

[37] J. Wiesner and A. Vilcinskas, "Antimicrobial peptides: The ancient arm of the human immune system," *Virulence,* vol. 1, no. 5, pp. 440-464, 2010.

[38] Y. Huan, Q. Kong, H. Mou and H. Yi, "Antimicrobial Peptides: Classification, Design, Application and Research Progress in Multiple Fields," *Frontiers in Microbiology,* vol. 11, p. 582779, 2020.

[39] Y. Zhang, F. B. L. Cougnon, Y. A. Wanniarachchi, J. A. Hayden and E. M. Nolan, "Reduction of Human Defensin 5 Affords a High-Affinity Zinc-Chelating Peptide," *ACS Chemical Biology,* vol. 8, no. 9, pp. 1907-1911, 2013.

[40] M. Mirouze, J. Sels, O. Richard, P. Czernic, S. Loubet, A. Jacquier, I. E. J. A. François, B. P. A. Cammue, M. Lebrun, P. Berthomieu and L. Marquès, "A putative novel role for plant defensins: a defensin from the zinc hyper-accumulating plant, Arabidopsis halleri, confers zinc tolerance," *The Plant Journal,* vol. 47, no. 3, pp. 329-342, 2006.

[41] M. R. Bleackley, S. Vasa, P. J. Harvey, T. M. A. Shafee, B. K. Kerenga, T. P. Soares da Costa, D. J. Craik, R. G. T. Lowe and M. A. Anderson, "Histidine-Rich Defensins from the Solanaceae and Brasicaceae Are Antifungal and Metal Binding Proteins," *Journal of Fungi,* vol. 6, no. 3, p. 145, 2020.

[42] S. D. Paredes, S. Kim, M. T. Rooney, A. I. Greenwood, K. Hristova and M. L. Cotten, "Enhancing the membrane activity of Piscidin 1 through peptide metallation and the presence of oxidized lipid species: Implications for the unification of host defense mechanisms at lipid membranes," *Biochimica et Biophysica Acta (BBA) - Biomembranes,* vol. 1862, no. 7, p. 183236, 2020.

[43] D. Łoboda, H. Kozłowski and M. Rowińska-Żyrek, "Antimicrobial peptide–metal ion interactions – a potential way of activity enhancement," *New Journal of Chemistry,* vol. 42, pp. 7560-7568, 2018.

[44] F. D. Silva, C. A. Rezende, D. C. Rossi, E. Esteves, F. H. Dyszy, S. Schreier, F. Gueiros-Filho, C. B. Campos, J. R. Pires and S. Daffre, "Structure and Mode of Action of Microplusin, a Copper II-chelating Antimicrobial Peptide from the Cattle Tick Rhipicephalus (Boophilus) microplus," *Journal of Biological Chemistry,* vol. 284, no. 50, pp. 34735-34746, 2009.

[45] L. M. Sabatini and E. A. Azen, "Histatins, a family salivary histidine-rich proteins, are encoded by at least two loci (HIS1 and HIS2)," *Biochemical and Biophysical Research Communications,* vol. 160, no. 2, pp. 495-502, 1989.

[46] H. Du, S. Puri, A. McCall, H. L. Norris, T. Russo and M. Edgerton, "Human Salivary Protein Histatin 5 Has Potent Bactericidal Activity against ESKAPE Pathogens," *Frontiers in Cellular and Infection Microbiology,* vol. 7, no. 41, 2017.

[47] P. A. Raj, E. Marcus and D. K. Sukumaran, "Structure of human salivary histatin 5 in aqueous and nonaqueous solutions," *Biopolymers,* vol. 45, no. 1, pp. 51-67, 1998.

[48] A. B. Mochon and H. Liu, "The antimicrobial peptide histatin-5 causes a spatially restricted disruption on the Candida albicans surface, allowing rapid entry of the peptide into the cytoplasm," *PLos Pathogens,* vol. 4, no. 10, p. e1000190, 2008.

[49] E. J. Helmerhorst, R. F. Troxler and F. G. Oppenheim, "The human salivary peptide histatin 5 exerts its antifungal activity through the formation of reactive oxygen species," *PNAS,* vol. 98, no. 25, pp. 14637-14642, 2001.

[50] S. Puri and M. Edgerton, "How Does it Kill?: Understanding the Candidacidal Mechanism of Salivary Histatin 5," *Eukaryotic Cell,* vol. 13, no. 8, pp. 958-964, 2014.

[51] H. Gusman, U. Lendenmann, J. Grogan, R. F. Troxler and F. G. Oppenheim, "Is salivary histatin 5 a metallopeptide?," *Biochimica et Biophysica Acta (BBA) - Protein Structure and Molecular Enzymology,* vol. 1545, no. 1-2, pp. 86-95, 2001.

[52] S. E. Conklin, E. C. Bridgman, Q. Su, P. Riggs-Gelasco, K. L. Haas and K. J. Franz, "Specific Histidine Residues Confer Histatin Peptides with Copper-Dependent Activity against Candida albicans," *Biochemistry,* vol. 56, no. 32, pp. 4244-4255, 2017.

[53] S. Puri, R. Li, D. Ruszaj, S. Tati and M. Edgerton, "Iron Binding Modulates Candidacidal Properties of Salivary Histatin 5," *Journal of Dental Research,* vol. 94, no. 1, pp. 201-208, 2015.

[54] H. L. Norris, R. Kumar, C. Y. Ong, D. Xu and M. Edgerton, "Zinc Binding by Histatin 5 Promotes Fungicidal Membrane Disruption in C. albicans and C. glabrata," *Journal of Fungi (Basel),* vol. 6, no. 3, p. 124, 2020.

[55] T. G. McCaslin, C. V. Pagba, J. Yohannan and B. A. Barry, "Specific metallo-protein interactions and antimicrobial activity in Histatin-5, an intrinsically disordered salivary peptide," *Scientific Reports,* vol. 9, p. 17303, 2019.

[56] M. J. Walker, T. C. Barnett, J. D. McArthur, J. N. Cole, C. M. Gillen, A. Henningham, K. S. Sriprakash, M. L. Sanderson-Smith and V. Nizet, "Disease manifestations and pathogenic mechanisms of Group A Streptococcus," *Clinical Microbiology Reviews,* vol. 27, no. 2, pp. 264-301, 2014.

[57] A. G. Turner, C.-L. W. M. J. Ong, K. Y. Djoko and A. G. McEwan, "Transition Metal Homeostasis in Streptococcus pyogenes and Streptococcus pneumoniae," *Advances in Mirobial Physiology,* vol. 70, pp. 123-191, 2017.

[58] A. J. Guerra, C. E. Dann III and D. P. Giedroc, "Crystal Structure of the Zinc-Dependent MarR Family Transcriptional Regulator AdcR in the Zn(II)-Bound State," *Journal of the American Chemical Society,* vol. 133, no. 49, pp. 19614-19617, 2011.

[59] C. E. Outten and T. V. O'Halloran, "Femtomolar Sensitivity ofMetalloregulatory ProteinsControlling Zinc Homeostasis," *Science,* vol. 292, no. 5526, pp. 2488-2492, 2001.

[60] M. Sanson, N. Makthal, A. R. Flores, R. J. Olsen, J. M. Musser and M. Kumaraswami, "Adhesin competence repressor (AdcR) from Streptococcus pyogenes controls adaptive responses to zinc limitation and contributes to virulence," *Nucleic Acids Research,* vol. 43, no. 1, pp. 418-432, 2015.

[61] V. Tedde, R. Rosini and C. L. Galeotti, "Zn2+ Uptake in Streptococcus pyogenes: Characterization of adcA and lmb Null Mutants," *PLoS One,* vol. 11, no. 3, p. e0152835, 2016.

[62] C.-l. Y. Ong, C. M. Gillen, T. C. Barnett, M. J. Walker and A. G. McEwan, "An Antimicrobial Role for Zinc in Innate Immune Defense Against Group A Streptococcus," *The Journal of Infectious Diseases,* vol. 209, no. 10, pp. 1500-1508, 2014.

[63] J. E. Martin, K. A. Edmonds, K. E. Bruce, G. C. Campanello, B. A. Eijkelkamp, E. B. Brazel, C. A. McDevitt, M. E. Winkler and D. P. Giedroc, "The zinc efflux activator SczA protects Streptococcus pneumoniae serotype 2 D39 from intracellular zinc toxicity," *Molecular Microbiology,* vol. 104, no. 4, pp. 636-651, 2017.

[64] A. Kandegedara, S. Thiyagarajan, K. C. Kondapalli, T. L. Stemmler and B. P. Rosen, "Role of Bound Zn(II) in the CadC Cd(II)/Pb(II)/Zn(II)-responsive Repressor," *Journal of Biological Chemistry,* vol. 284, no. 22, pp. 14958-14965, 2009.

[65] Z. Luo, J. R. Morey, E. Deplazes, A. Motgullina, A. Tan, K. Ganio, S. L. Neville, N. Eleftheriadis, M. Isselstein, V. G. Pederick, J. C. Paton, T. Cordes and J. R. Harmer, "A Trap-Door Mechanism for Zinc Acquisition by Streptococcus pneumoniae AdcA," *Bacteriology,* vol. 12, no. 1, pp. e01958-20, mBio.

[66] K. Cao, N. Li, H. Wang, X. Cao, J. He, B. Zhang, Q.-Y. He, G. Zhang and X. Sun, "Two zinc-binding domains in the transporter AdcA from Streptococcus pyogenes facilitate high-affinity binding and fast transport of zinc," *Journal of Biological Chemistry,* vol. 293, no. 16, pp. 6075-6089, 2018.

[67] M. L. Župan, Z. Luo, K. Ganio, V. G. Pederick, S. L. Neville, E. Deplazes, B. Kobe and C. A. McDevitt, "Conformation of the Solute-Binding Protein AdcAII Influences Zinc Uptake in Streptococcus pneumoniae," *Frontiers in Cellular and Infection Microbiology,* vol. 11, p. 729981, 2021.

[68] C.-l. Y. Ong, O. Berking, M. J. Walker and A. G. McEwan, "New Insights into the Role of Zinc Acquisition and Zinc Tolerance in Group A Streptococcal Infection," *Infection and Immunity,* Vols. 86:e00048-18, 2018.

[69] J. E. Martin and D. P. Giedroc, "Functional Determinants of Metal Ion Transport and Selectivity in Paralogous Cation Diffusion Facilitator Transporters CzcD and MntE in Streptococcus pneumoniae," *Journal of Bacteriology,* vol. 198, no. 7, pp. 1066-1076, 2016.

[70] T. G. V. D. K.-P. M. M. Kloosterman, J. J. E. Bijlsma and O. P. Kuipers, "The novel transcriptional regulator SczA mediates protection against Zn2+ stress by activation of the Zn2+-resistance gene czcD in Streptococcus pneumoniae," *Molecular Microbiology,* vol. 65, no. 4, pp. 1049-1063, 2007.

[71] B. Weston, A. Brenot and M. G. Caparon, "The Metal Homeostasis Protein, Lsp, of Streptococcus pyogenes Is Necessary for Acquisition of Zinc and Virulence," *American Society for Microbiology,* vol. 77, no. 7, pp. 2840-2848, 2009.

[72] C.-l. Y. Ong, M. J. Walker and A. G. McEwan, "Zinc disrupts central carbon metabolism and capsule biosynthesis in Streptococcus pyogenes," *Scientific Reports,* vol. 5, p. 10799, 2015.

[73] G. H. Stollerman and J. B. Dale, "The Importance of the Group A Streptococcus Capsule in the Pathogenesis of Human Infections: A Historical Perspective," *Clinical Infectious Diseases,* vol. 46, no. 7, pp. 1038-1045, 2008.

[74] K. C. Krishnan, S. Mukundan, J. A. L. Figueroa, J. A. Caruso and M. Kotb, "Metal-Mediated Modulation of Streptococcal Cysteine Protease Actvity and Its Biological Implications," *American Society for Microbiology,* vol. 82, no. 7, pp. 2992-3001, 2014.

[75] R. K. Aziz, M. J. Pabst, A. Jeng, R. Kansal, D. E. Low, V. Nizet and M. Kotb, "Invasive M1T1 group A Streptococcus undergoes a phase-shift in vivo to prevent proteolytic degradation of multiple virulence factors by SpeB," *Molecular Microbiology,* vol. 51, no. 1, pp. 123-134, 2003.

[76] C. A. Young, L. D. Gordon, Z. Fang, R. C. Holder and S. D. Reid, "Copper Tolerance and Characterization of a Copper-Responsive Operon, copYAZ, in an M1T1 Clinical Strain of Streptococcus pyogenes," *Journal of Bacteriology,* vol. 197, no. 15, pp. 2580-2592, 2015.

[77] H. Glauninger, Y. Zhang, K. A. Higgins, A. D. Jacobs, J. E. Martin, Y. Fu, H. J. Coyne 3rd, K. E. Bruce, M. J. Maroney, D. E. Clemmer, D. A. Capdevila and D. P. Giedroc, "Metal-dependent allosteric activation and inhibition on the same molecular scaffold: the copper sensor CopY from Streptococcus pneumoniae," *Chemical Science,* vol. 9, pp. 105-118, 2017.

[78] S. Ekici, H. Yang, H.-G. Koch and F. Daldal, "Novel Transporter Required for Biogenesis of cbb3-Type Cytochrome c Oxidase in Rhodobacter capsulatus," *mBio,* vol. 3, no. 1, pp. e00293-11, 2012.

[79] G. E. Kenney and A. C. Rosenzweig, "Chalkophores," *Annual Review of Biochemistry,* vol. 87, pp. 645-676, 2018.

[80] H. Al-Tameemi, W. N. Beavers, J. Norambuena, E. P. Skaar and J. M. Boyd, "Staphylococcus aureus lacking a functional MntABC manganese import system has increased resistance to copper," *Molecular Microbiology,* vol. 115, no. 4, pp. 554-573, 2021.

[81] R. Janulczyk, J. Pallon and L. Biörck, "Identification and characterization of a Streptococcus pyogenes ABC transporter with multiple specificity for metal cations," *Molecular Microbiology,* vol. 34, no. 3, pp. 596-606, 1999.

[82] S. Shafeeq, H. Yesilkaya, T. G. Kloosterman, G. Narayanan, M. Wandel, P. W. Andrew, O. P. Kuipers and J. A. Morrissey, "The cop operon is required for copper homeostasis and contributes to virulence in Streptococcus pneumoniae," *Molecular Microbiology,* vol. 81, no. 5, pp. 1255-1270, 2011.

[83] L. J. Stewart, C.-l. Ong, M. M. Zhang, S. Brouwer, L. McIntyre, M. R. Davies, M. J. Walker, A. G. McEwan, K. J. Waldron and K. Y. Djoko, "Role of glutathione in buffering excess intracellular copper in Streptococcus pyogenes," *mBio,* vol. 11, no. 6, pp. e02804-20, 2020.

[84] W. Maret and B. L. Vallee, "Thiolate ligands in metallothionein confer redox activity on zinc clusters," *PNAS,* vol. 95, no. 7, pp. 3478-3482, 1998.

[85] T. J. B. Simons, "Measurement of free Zn2+ ion concentration with the fluorescent probe mag-fura-2 (furaptra)," *Journal of Biochemical and Biophysical Methods,* vol. 27, no. 1, pp. 25-37, 1993.

[86] J. R. Jefferson, J. B. Hunt and A. Ginsburg, "Characterization of indo-1 and quin-2 as spectroscopic probes for Zn2+ -protein interactions," *Analytical Biochemistry,* vol. 187, no. 2, pp. 328-336, 1990.

[87] K. R. Gee, Z.-L. Zhou, W.-J. Qian and R. Kennedy, "Detection and Imaging of Zing Secretion from Pancreatic β-Cells Using a New Fluorescent Zinc Indicator," *Journal of the American Chemical Society,* vol. 124, no. 5, pp. 776-778, 2002.

[88] M. Zimmermann, O. Clarke, J. M. Gulbis, D. W. Keizer, R. S. Jarvis, C. S. Cobbett, M. G. Hinds, Z. Xiao and A. G. Wedd, "Metal Binding Affinities of Arabidopsis Zinc and Copper Transporters: Selectivities Match the Relative, but Not the Absolute, Affinities of their Amino-Terminal Domains,," *Biochemistry,* vol. 48, no. 49, pp. 11640-11654, 2009.

[89] Z. Xiao, P. S. Donnelly, M. Zimmermann and A. G. Wedd, "Transfer of Copper between Bis(thiosemicarbazone) Ligands and Intracellular Copper-Binding Proteins. Insights into Mechanisms of Copper Uptake and Hypoxia Selectivity," *Inorganic Chemistry,* vol. 47, no. 10, pp. 4338-4347, 2008.

[90] J. Zhao, B. A. Bertoglio, M. J. Devinney Jr, K. E. Dineley and A. R. Kay, "The interaction of biological and noxious transition metals with the zinc probes FluoZin-3 and Newport Green," *Analytical Biochemistry,* vol. 384, no. 1, pp. 34-41, 2009.

[91] C. S. Atwood, R. C. Scarpa, X. Huang, R. D. Moir, W. D. Jones, D. P. Fairlie, R. E. Tanzi and A. I. Bush, "Characterization of Copper Interactions with Alzheimer Amyloid β Peptides," *Journal of Neurochemistry,* vol. 75, no. 3, pp. 1219-1233, 2008.

[92] C. J. Sarell, C. D. Syme, S. E. J. Rigby and J. H. Viles, "opper(II) Binding to Amyloid-β Fibrils of Alzheimer's Disease Reveals a Picomolar Affinity: Stoichiometry and Coordination Geometry Are Independent of Aβ Oligomeric Form," *Biochemistry,* vol. 48, no. 20, pp. 4388-4402, 2009.

[93] L. J. Stewart, C.-l. Ong, M. M. Zhang, S. Brouwer, L. McIntyre, M. R. Davies, M. J. Walker, A. G. McEwan, K. J. Waldron and K. Y. Djoko, "Role of glutathione in buffering excess intracellular copper in Streptococcus pyogenes," *mBio,* vol. 11, no. 6, pp. e02804-20, 2020.

[94] S. Chatellier, N. Ihendyane, R. G. Kansal, F. Khambaty, H. Basma, A. Norrby-Teglund, D. E. Low, A. McGeer and M. Kotb, "Genetic Relatedness and Superantigen Expression in Group A Streptococcus Serotype M1 Isolates from Patients with Severe and Nonsevere Invasive Diseases," *American Society For Microbiology,* vol. 68, no. 6, pp. 3523-3534, 2000.

[95] C.-l. Y. Ong, C. M. Gillen, T. C. Barnett, M. J. Walker and A. G. McEwan, "An Antimicrobial Role for Zinc in Innate Immune Defense Against Group A Streptococcus," *The Journal of Infectious Disease,* vol. 209, no. 10, pp. 1500-1508, 2014.

[96] A. Kocyła, A. Pomorski and A. Krężel, "Molar absorption coefficients and stability constants of Zincon metal complexes for determination of metal ions and bioinorganic applications," *Journal of Inorganic Biochemistry,* vol. 176, pp. 53-65, 2017.

[97] E. Loisel, L. Jacquamet, L. Serre, C. Bauvois, J. L. Ferrer, V. Thierry, A. M. D. Guilmi and C. Durmort, "AdcAII, a new pneumococcal Zn-binding protein homologous with ABC transporters: biochemical and structural analysis," *Journal of Molecular Biology,* vol. 381, no. 3, pp. 594-606, 2008.

[98] L. Stewart, Y. Hong, I. Holmes, S. Firth, J. Bolton, Y. Santos, S. Cobb, N. Jakubovics and K. Djoko, "The salivary, metal-binding peptide histatin-5 buffers extracellular copper availability," *bioRxiv ,* vol. 2022.01.07. 472205 , no. doi: https://doi.org/10.1101/2022.01.07.472205, [cited 2022 Mar].

[99] T. R. Young and Z. Xiao, "Principles and practice of determining metal-protein affinities," *Biochemical Journal,* vol. 478, pp. 1085-1116, 2021.

[100] A. Krężel and W. Maret, "The biological inorganic chemistry of zinc ions," *Archives of Biochemistry and Biophysics ,* vol. 611, pp. 3-19, 2016.

[101] E. Kurowska, A. Bonna, G. Goch and W. Bal, "Salivary histatin-5, a physiologically relavant ligand for Ni(II) ions," *Journal of Inorganic Biochemistry,* vol. 105, no. 9, pp. 1220-1225, 2011.

[102] E. Loisel, S. Chimalapati, C. Bougault, A. Imberty, B. Gallet, A. M. D. Guilmi, J. Brown, T. Vernet and C. Durmort, "Biochemical Characterization of the Histidine Triad Protein PhtD as a Cell Surface Zinc-Binding Protein of Pneumococcus," *Biochemistry,* vol. 50, no. 17, pp. 3551-3558, 2011.

[103] A. Elsner, B. Kreikemeyer, A. Braun-Kiewnick, B. Spellerberg, B. A. Buttaro and A. Podbielski, "Involvement of Lst, a Member of the LraI-Lipoprotein Family in Streptococcus pyogenes, in Eukaryotic Cell Adhesion and Internalization," *American Society for Microbiology,* vol. 70, no. 9, pp. 4859-4869, 2002.